

Signal design for MIMO dual-function systems with permutation learning

Jing YANG^{2,1}, Xianxiang YU¹, Minghui SHA³, Wen FAN⁴ & Guolong CUI^{1*}

¹*School of Information and Communication Engineering, University of Electronic Science and Technology of China, Chengdu 611731, China;*

²*School of Electrical and Information Engineering, Zhengzhou University, Zhengzhou 450001, China;*

³*Beijing Institute of Radio Measurement, Beijing 100854, China;*

⁴*The 54th Research Institute of China Electronics Technology Group Corporation, Shijiazhuang 050081, China*

Received 5 June 2022/Revised 12 October 2022/Accepted 12 December 2022/Published online 25 September 2023

Abstract This paper addresses the signal matrix synthesis in the multi-input-multi-output (MIMO) dual-function system aimed at obtaining the desired radar beampattern while embedding communication symbols into the permutation matrix of each pulse. To this end, transmit beampattern peak mainlobe to sidelobe level ratio (PMSR) is considered the figure of merit. Besides, the phases of the codebook induced by the designed weight vectors impinging on the directions of the communication receivers and eavesdroppers are restricted to be uniformly distributed and totally the same, respectively. To handle the resulting design problem, an iterative algorithm is devised to account for the coupled quadratic fractional programming objective function with multi-equality constraints, capitalizing on the alternating direction method of multipliers (ADMM) framework. As to the demodulation process for permutation learning, a novel algorithm based on the alternating direction penalty method (ADPM) framework is proposed to handle the mix-boolean optimization problem with the correlation between the communication dictionary and permutation of the received filtered data maximized. Finally, numerical results highlight the effectiveness of the conceived algorithms in comparison with the existing counterparts.

Keywords dual function radar and communication (DFRC) system, multi-input multi-output (MIMO) radar beampattern, alternating direction method of multipliers (ADMM), permutation learning, mix-boolean optimization problem, alternating direction penalty method (ADPM)

Citation Yang J, Yu X X, Sha M H, et al. Signal design for MIMO dual-function systems with permutation learning. *Sci China Inf Sci*, 2023, 66(10): 202303, <https://doi.org/10.1007/s11432-022-3651-8>

1 Introduction

With increasing demands on high-resolution radar sensing and communication, competition for the limited radio frequency (RF) spectrum prompts the development of co-existence and co-design methods for spectral congestion [1–5]. Therein, the dual-function radar communication (DFRC) system with co-use waveforms has drawn much attention by virtue of the advantage in miniaturization, module, and efficiency in spectral resources on an emerging platform [6]. It finds applications in various areas, such as smart transit systems with the vehicular network, the Internet of things (IoT), unmanned aerial vehicles, and military equipment [7–9]. Compared with the phased array counterpart, the multi-input multi-output (MIMO) system provides more degrees of freedom (DoFs) in terms of waveform diversity and radar beam [10–13], which both can be the carrier of the communication information. In this respect, a plethora of papers in the open literature have focused on the construction of MIMO DFRC frameworks and the synthesis of integrated waveforms.

For the multi-carrier MIMO system, frequency hopping (FH) and orthogonal frequency division multiplexing (OFDM) signals are broadly used [14–16]. In [17], each frequency hop is multiplied by the phase shift keying (PSK) communication symbol, whereas the code shift keying (CSK) embedding strategy is employed in [18–20]. Therein, Ref. [18] modulated the phase-coded sequence by the continuous phase

* Corresponding author (email: cuiquolong@uestc.edu.cn)

modulation (CPM) for range sidelobe levels reduction and good spectrum containment. Furthermore, Ref. [21] relaxed the orthogonality constraint between different FH waveforms to increase the data rate and optimize the joint radar and communication (JRC) performance. In [22], the data rate is increased via the spatial modulation for embedding communication symbols. Besides, OFDM communication signal is performed in [23] for radar measurements applied in vehicular networks. Ref. [24] synthesized a phase-coded OFDM signal and associated processing technique to obtain higher resolution in radar estimation, while Ref. [25] offered a JRC fusion system framework with constant envelope OFDM signal. In addition, the frequency diverse array (FDA)-MIMO framework for JRC systems is also considered, where the communication symbols can be embedded into the frequency increment [26], beampattern [27], Costas sequence modulated frequency offsets [28], etc.

As to single carrier MIMO system, one approach is to design communication-centric precoders for transmit beamforming from the multi-antenna base station (BS) to support radar sensing, where the channels from BS to the users are modeled by stochastic distributions. Ref. [29] proposed beamforming techniques for the MIMO JRC system with both separated and shared antenna deployments while guaranteeing the signal to interference plus noise ratio (SINR) and power budget at the intended users. In [30], the multi-user interference (MUI) is minimized with an appropriate radar beampattern formulated via a similarity constraint, where the developed framework is further extended to the range sidelobe suppression for radar performance improvement in [31]. Along this line, to optimize the weighted sum of MUI energy and radar receive SINR, Ref. [32] tackled the joint transceiver design, where different spatial/temporal constraints, like total transmit energy, constant-modulus, and similarity constraints, are considered at the signal design process, respectively. Furthermore, Ref. [33] employed symbol-level precoding techniques so as to obtain more degrees of freedom for better JRC performance.

Another line focuses on the information embedding for radar-centric DFRC MIMO systems with beam-space channel model [34], which is also concerned in this paper. Therein, adopting a linear combination of the individual orthogonal waveforms, beamforming weight vectors are synthesized for the JRC function, where a communication channel with an intrinsic geometric structure is involved. Specifically, amplitude shift keying (ASK) [35], PSK [36], and quadrature amplitude modulation (QAM) [37] techniques are exploited, respectively, to embed the information into the MIMO radar beampattern for multi-users. Besides, in [38], the permutation matrix is employed shuffling the independent waveforms across the transmit antennas, which is transparent to the beampattern while conveying information. Ref. [39] further extended to the joint modulation via waveform permutation and antenna allocation to obtain a higher data rate. The communication receiver decodes the transmitted information by recovering the shuffling order. However, Refs. [38, 39] were only applicable to one communication receiver.

In this paper, we focus on the signal matrix design for desired beamforming in DFRC MIMO systems, where the permutation matrix transparent to the beampattern is adopted for information embedding. Specifically, unlike the previous study [38], the peak mainlobe to sidelobe level ratio (PMSR) of transmit beampattern is considered the figure of merit without specifying pattern masks. Moreover, the phase distribution constraints are performed on the codebooks of assigned directions to deal with multi-users and eavesdroppers at the same time. To tackle the resulting quadratic fractional programming problem, an iterative procedure leveraging the alternating direction method of multipliers (ADMM) is conceived, which can quickly converge to an optimized solution under some mild conditions. Specifically, auxiliary variables are introduced to decouple the numerator, denominator, and multi-equality constraints, where a closed-form optimal solution to each convex subproblem can be derived in each iteration with comparatively low computational complexity. Moreover, a novel iterative algorithm resorting to the alternating direction penalty method (ADPM) framework is proposed for the demodulation process of permutation learning, which solves the resulting mix-boolean optimization problem with the computational complexity polynomial with respect to the number of beamforming weight vectors, which conquers the demodulation failure brought by the exhaustive search with the massive possibility of symbols in each pulse. To shed light on the capability of the devised algorithms to ensure dual function, some case studies are provided at the analysis stage. Moreover, appropriate comparisons with some counterparts available in the open literature are presented to prove the effectiveness of the new proposed algorithms.

The paper is organized as follows. In Section 2, the system model is introduced, including the radar transmit and user receive signal models, modulation rule as well as innovative demodulation optimization methods. In Section 3, the DFRC signal design problem is formulated with the key performance metric as well as constraints involved. An iterative algorithm leveraging ADMM is devised to tackle the resulting quadratic fractional programming optimization problem. Section 4 presents some numerical results to

assess the performance. Finally, in Section 5, concluding remarks and some possible future research avenues are provided.

Notations. Bold letters, e.g., \mathbf{a} (lower case) and \mathbf{A} (upper case) denote vector and matrix, respectively. $(\cdot)^T$ and $(\cdot)^\dagger$ denote the transpose and the conjugate transpose operators, respectively. $\mathbb{C}^{N \times M}$, \mathbb{R}^N , \mathbb{C}^N are, respectively, the sets of $N \times M$ -dimensional matrices of complex, N -dimensional vectors of real and complex numbers. $\|\mathbf{x}\|$ denotes the Euclidean norm. \mathbf{I}_N denotes the $N \times N$ -dimensional identity matrix. $\mathbf{1}_N \in \mathbb{R}^N$ is a vector with all entries being 1. \mathbf{e}_n is a vector whose n -th entry is 1 and other elements are 0. Letter j represents the imaginary unit (i.e., $j = \sqrt{-1}$). $\Re\{\cdot\}$ and $\Im\{\cdot\}$ are the real and imaginary parts of a complex number, respectively. $\arg(\cdot)$ and $|\cdot|$ mean the argument and modulus of a complex valued scalar, vector, or matrix. $\lfloor \cdot \rfloor$ denotes the operation of rounding down to the nearest integer. $\text{tr}(\mathbf{A})$ is the trace of the square matrix \mathbf{A} .

2 System model

This section focuses on the DFRC system model in terms of the transmit signal model with information modulation criterion, the beampattern for the primary radar function, the corresponding receive signal of each user equipment (UE), and the demodulation for the secondary communication function.

2.1 Transmit signal model and information embedding

A narrowband DFRC radar system with M omnidirectional colocated transmit antennas in a uniform linear array (ULA) with inter-element spacing d is considered. Let $\Phi = [\phi_1, \phi_2, \dots, \phi_K]^T \in \mathbb{C}^{K \times L}$ be the matrix of orthogonal discrete waveform sets $\{\phi_k\}_{k=1}^K$ with the number of snapshots in each pulse L . Assuming that $\{\phi_k\}_{k=1}^K$ satisfy the orthogonality condition at all time-delays and Doppler-shifts within the range and velocity specifications¹⁾, it follows that

$$\Phi \Phi^\dagger = \mathbf{I}_K. \quad (1)$$

To embed information into the MIMO radar emission, a permutation matrix $\mathbf{P}_i = [e_{f_{i,1}}, e_{f_{i,2}}, \dots, e_{f_{i,K}}]^T \in \mathbb{R}^{K \times K}$, $i \in \{1, \dots, K\}$, is employed to shuffle the pre-designed waveform sets [38] with the one-to-one mapping: $k \in \{1, \dots, K\} \rightarrow f_{i,k} \in \{1, \dots, K\}$, which satisfies

$$\mathbf{P}_i \mathbf{P}_i^T = \mathbf{P}_i^T \mathbf{P}_i = \mathbf{I}_K. \quad (2)$$

The reconstructed orthogonal waveform sets in i -th pulse can be expressed as

$$\Psi_i = \mathbf{P}_i \Phi = [\phi_{f_{i,1}}, \phi_{f_{i,2}}, \dots, \phi_{f_{i,K}}]^T. \quad (3)$$

Hence, the embedded information for a single pulse is

$$E = \lfloor \log_2(K) \rfloor \text{ bits}. \quad (4)$$

Furthermore, according to the signaling scheme shown in Figure 1, the weight matrix $\mathbf{W} = [\mathbf{w}_1, \dots, \mathbf{w}_K] \in \mathbb{C}^{M \times K}$ is adopted to linearly combine Ψ_i for the energy distribution of transmit beampattern, where $\mathbf{w}_k \in \mathbb{C}^M$, $k \in \{1, \dots, K\}$, denotes the weight vector of M transmit antennas for the k -th orthogonal waveform. In this respect, the l -th snapshot signal at the input of M transmit antennas can be written as

$$\bar{\mathbf{s}}(l) = \sum_{k=1}^K \mathbf{w}_k \phi_{f_{i,k}}(l) \in \mathbb{C}^M \quad (5)$$

with $\phi_{f_{i,k}}(l)$, the l -th element of $\phi_{f_{i,k}}$.

Consequently, the baseband representation of the transmit signal matrix is

$$\mathbf{S}_i = [\bar{\mathbf{s}}(1), \dots, \bar{\mathbf{s}}(L)] = \mathbf{W} \Psi_i \in \mathbb{C}^{M \times L}. \quad (6)$$

1) Although perfectly orthogonal waveforms with overlapped spectrum cannot be realized, waveforms with low cross-correlations, e.g., OFDM waveforms and phase-coded waveforms can be adopted [38, 40, 41].

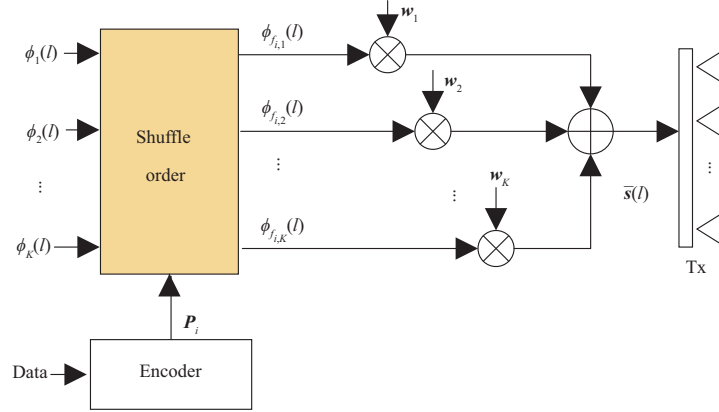


Figure 1 (Color online) Signaling scheme of the DFRC MIMO system.

2.2 Transmit beampattern for radar detection

Assuming that the propagation is nondispersive, the synthesized signal at a target direction θ of the i -th pulse is

$$\mathbf{y}_i(\theta) = (\mathbf{a}^\dagger(\theta)\mathbf{S}_i)^\mathbf{T}, \quad (7)$$

where $\mathbf{a}(\theta)$ is the transmit spatial steering vector, given by

$$\mathbf{a}(\theta) = \left[1, e^{j2\pi\frac{d}{\lambda}\sin\theta}, \dots, e^{j2\pi\frac{(M-1)d}{\lambda}\sin\theta} \right]^\mathbf{T} \quad (8)$$

with λ denoting the wavelength. The power for the probing signal at location θ , i.e., the transmit beampattern, can be written as

$$P(\theta) = \|\mathbf{a}^\dagger(\theta)\mathbf{S}_i\|^2 = \|\mathbf{a}^\dagger(\theta)\mathbf{W}\|^2 = \|\mathbf{A}^\dagger(\theta)\mathbf{w}\|^2, \quad (9)$$

where $\mathbf{w} = \text{vec}(\mathbf{W})$, $\mathbf{A}(\theta) = \mathbf{I}_K \otimes \mathbf{a}(\theta)$. To restrict the total transmit energy in a single pulse, let us restrict $E_t = \text{tr}(\mathbf{W}^\dagger\mathbf{W}) = \|\mathbf{w}\|^2 = \Delta$. Note that $P(\theta)$ is irrelevant with \mathbf{P}_i ; namely, the transmission of communication information is transparent to the beampattern.

2.3 Receive signal model for communication

Suppose that \mathbf{S}_i is transmitted in the i -th pulse and there are C single-antenna communication users as shown in Figure 2 located at the direction of θ_c^{com} , $c = 1, \dots, C$, respectively. The baseband observation of the c -th communication receiver can be modeled as

$$\mathbf{r}_c^i = \alpha_c^i (\mathbf{a}^\dagger(\theta_c^{\text{com}})\mathbf{S}_i)^\mathbf{T} + \mathbf{n}_c^i \in \mathbb{C}^L, \quad (10)$$

where α_c^i , $c = 1, \dots, C$, is the channel coefficient of the i -th pulse representing the propagation environment between the MIMO radar transmit array and the c -th communication receiver²⁾, and \mathbf{n}_c^i is a noise additive term which is modeled as a complex, zero-mean, circularly symmetric Gaussian random vector.

Then, let the received data \mathbf{r}_c^i matched filtering to Φ , which yields

$$\mathbf{x}_c^i = \Phi^* \mathbf{r}_c^i = \alpha_c^i \mathbf{P}_i^\mathbf{T} \mathbf{s}(\theta_c^{\text{com}}) + \hat{\mathbf{n}}_c^i, \quad (11)$$

where $\hat{\mathbf{n}}_c^i = \Phi^* \mathbf{n}_c^i$ is the additive noise term after matched filtering with covariance $\sigma_n^2 \mathbf{I}_K$, and

$$\mathbf{s}(\theta) = (\mathbf{a}^\dagger(\theta)\mathbf{W})^\mathbf{T} = \mathbf{A}^\dagger(\theta)\mathbf{w}, \quad (12)$$

satisfies $P(\theta) = \|\mathbf{s}(\theta)\|^2$.

²⁾ Let us assume that the channel is estimated accurately and non-changing. Pilot signals known to both the users and DFRC systems can be transmitted periodically for the channel state information estimation [38].

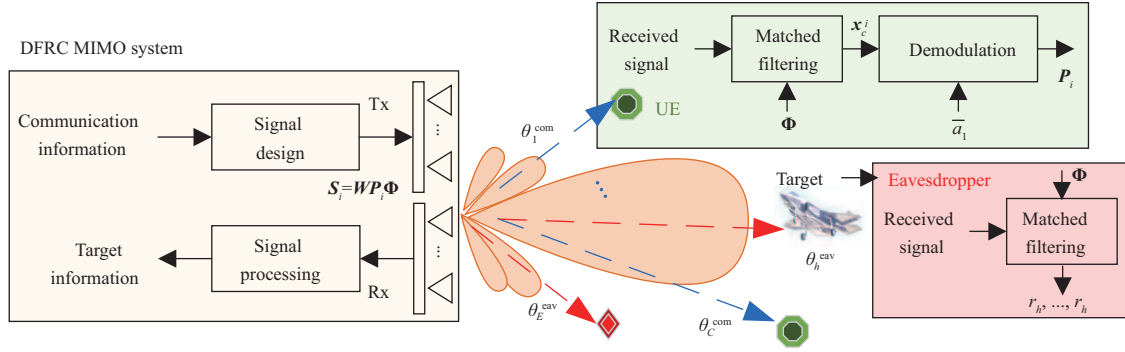


Figure 2 (Color online) Work scenario of MIMO DFRC system.

It can be observed that Eq. (11) is a scaled and noisy shuffling of $\mathbf{s}(\theta_c^{\text{com}})$, where $\mathbf{s}(\theta_c^{\text{com}})$ plays the role of codebook for communication. Hence, the demodulation process at each UE's receiver end is to recover \mathbf{P}_i by comparing the elements of \mathbf{x}_c^i and $\mathbf{s}(\theta_c^{\text{com}})$ and determining the permutation order. To this end, it is necessary to make each element of $\mathbf{s}(\theta_c^{\text{com}})$ distinguish from each other. Without loss of generality, let us assign $\mathbf{s}(\theta_c^{\text{com}})$ to be PSK modulated, i.e.,

$$\mathbf{s}(\theta_c^{\text{com}}) = b_c \bar{\mathbf{a}}_1, \quad c = 1, \dots, C, \quad (13)$$

with $b_c \in \mathbb{R}$, the amplitude of $\mathbf{s}(\theta_c^{\text{com}})$ and $\bar{\mathbf{a}}_1 = [1, e^{j\frac{2\pi}{K}}, \dots, e^{j\frac{2\pi(K-1)}{K}}]^T$.

Furthermore, the radar targets and UEs with other communication tasks or seized by the enemy are considered potential eavesdroppers which locate at $\theta_h^{\text{eav}}, h = 1, \dots, E$ at the current pulse as shown in Figure 2. To prevent eavesdroppers from intercepting the communication message for enabling physical layer secrecy, the entries of $\mathbf{s}(\theta_h^{\text{eav}})$ are set all the same, i.e.,

$$\mathbf{s}(\theta_h^{\text{eav}}) = r_h \mathbf{1}_K, \quad h = 1, \dots, E, \quad (14)$$

with $r_h \in \mathbb{C}$, the value of the entries in $\mathbf{s}(\theta_h^{\text{eav}})$. As a result, even if the eavesdroppers have the precise knowledge of Φ and $\bar{\mathbf{a}}_1$, elements of the vector after matched filtering are all the same, which result in the demodulation failure.

2.4 Demodulation method

Assume that each communication receiver has perfect knowledge of orthogonal waveforms Φ and $\bar{\mathbf{a}}_1$. The demodulation process can be modeled as finding a permutation matrix \mathbf{P} via solving the following optimization problem [38]:

$$\begin{aligned} \min_{\mathbf{P}} \quad & \left\| \mathbf{x}_c^i - \mathbf{P}^T \mathbf{s}(\theta_c^{\text{com}}) \right\|^2 \\ \text{s.t.} \quad & \mathbf{P} \in \Lambda, \end{aligned} \quad (15)$$

where $\Lambda = \{\mathbf{P} | \mathbf{P}(i, j) \in \{0, 1\}, \mathbf{P}\mathbf{1}_K = \mathbf{1}_K, \mathbf{P}^T \mathbf{1}_K = \mathbf{1}_K\}$ defines a set of permutation matrices.

Note that Problem (15) is a mixed-boolean problem, which is solved by an exhaustive search in [38] and it fails to work when K is large³⁾. In this respect, a novel iterative mixed-boolean optimization method invoking ADPM is proposed.

As the first step toward this goal, let us re-parameterize the objective function as

$$\left\| \mathbf{x}_c^i - \mathbf{P}^T \mathbf{s}(\theta_c^{\text{com}}) \right\|^2 = -2b_c \Re\{\bar{\mathbf{a}}_1^\dagger \mathbf{P} \mathbf{x}_c^i\} + b \quad (16)$$

$$= -2b_c \mathbf{g}^T \mathbf{p} + b, \quad (17)$$

where $b = \|\mathbf{x}_c^i\|^2 + Kb_c^2$, $\mathbf{g} = \Re\{\mathbf{x}_c^i \otimes \bar{\mathbf{a}}_1^*\} \in \mathbb{R}^{K^2}$, $\mathbf{p} = \text{vec}(\mathbf{P}) \in \mathbb{R}^{K^2}$. Interestingly, Eq. (16) reveals that the demodulation can be observed as finding a permutation matrix to maximize the correlation between the dictionary $\bar{\mathbf{a}}_1$ and the shuffling of \mathbf{x}_c^i (i.e., $\mathbf{P}\mathbf{x}_c^i$).

3) The total numbers of symbols for $K = 4, 8, 16$ are $4! = 24$, $8! = 40320$ and $16! > 2 \times 10^{13}$, respectively, which is large although K is small. Therefore, Ref. [38] only chose 16 among $K!$ symbols to analyze the communication performance in the numerical simulation.

Furthermore, introducing auxiliary variables $\mathbf{q}_1, \mathbf{q}_2 \in \mathbb{R}^{K^2}$, Eq. (15) can be equivalently recast as

$$\begin{aligned} & \min_{\mathbf{p}} -\mathbf{g}^T \mathbf{p} \\ & \text{s.t. } p_i \in \{0, 1\}, i = 1, \dots, K^2, \\ & \quad \mathbf{q}_1 = \mathbf{p}, \\ & \quad \mathbf{B}\mathbf{q}_1 = \mathbf{1}_K, \\ & \quad \mathbf{q}_2 = \mathbf{p}, \\ & \quad \mathbf{C}\mathbf{q}_2 = \mathbf{1}_K, \end{aligned} \tag{18}$$

with $\mathbf{B} = \mathbf{1}_K^T \otimes \mathbf{I}_K$ and $\mathbf{C} = \mathbf{I}_K \otimes \mathbf{1}_K^T$. Hence, the augmented Lagrangian is defined as

$$\mathcal{L}_\rho(\mathbf{p}, \mathbf{q}_1, \mathbf{q}_2, \boldsymbol{\kappa}_1, \boldsymbol{\kappa}_2) = -\mathbf{g}^T \mathbf{p} + \frac{\rho}{2} \left\| \mathbf{q}_1 - \mathbf{p} + \frac{\boldsymbol{\kappa}_1}{\rho} \right\|^2 + \frac{\rho}{2} \left\| \mathbf{q}_2 - \mathbf{p} + \frac{\boldsymbol{\kappa}_2}{\rho} \right\|^2. \tag{19}$$

Let $\mathbf{p}^l, \mathbf{q}_1^l, \mathbf{q}_2^l, \boldsymbol{\kappa}_1^l, \boldsymbol{\kappa}_2^l, \rho^l$ denote the l -th iteration values of $\mathbf{p}, \mathbf{q}_1, \mathbf{q}_2, \boldsymbol{\kappa}_1, \boldsymbol{\kappa}_2, \rho$. The ADPM procedure is reported in Algorithm 1. Note that Problem (18) is prone to fall into a local optimum as it is a mixed Boolean optimization problem. In this respect, let us increase the penalty parameter ρ if $\|\mathbf{p}^{l+1} - \mathbf{p}^l\| = 0$ to strengthen the constraints on the original and auxiliary variables and accelerate the convergence.

Algorithm 1 ADPM algorithm for \mathcal{P}_1

Require: $\mathbf{p}^0, \mathbf{q}_1^0, \mathbf{q}_2^0, \boldsymbol{\kappa}_1^0, \boldsymbol{\kappa}_2^0, \rho^0, \mathbf{g}, \mathbf{B}, \mathbf{C}, \eta_1$;

Ensure: An optimized solution \mathbf{p}^* to Problem (18);

1: $l = 0$;

2: Update $\mathbf{p}^{l+1}, \mathbf{q}_1^{l+1}, \mathbf{q}_2^{l+1}$ by solving the following problems:

$$\begin{aligned} \mathbf{p}^{l+1} & := \arg \min_{\mathbf{p}} \mathcal{L}_\rho(\mathbf{p}, \mathbf{q}_1^l, \mathbf{q}_2^l, \boldsymbol{\kappa}_1^l, \boldsymbol{\kappa}_2^l) \\ & \text{s.t. } p_i \in \{0, 1\}, i = 1, \dots, K^2, \end{aligned} \tag{20}$$

$$\begin{aligned} \mathbf{q}_1^{l+1} & := \arg \min_{\mathbf{q}_1} \mathcal{L}_\rho(\mathbf{p}^{l+1}, \mathbf{q}_1, \mathbf{q}_2^l, \boldsymbol{\kappa}_1^l, \boldsymbol{\kappa}_2^l) \\ & \text{s.t. } \mathbf{B}\mathbf{q}_1 = \mathbf{1}_K, \end{aligned} \tag{21}$$

$$\begin{aligned} \mathbf{q}_2^{l+1} & := \arg \min_{\mathbf{q}_2} \mathcal{L}_\rho(\mathbf{p}^{l+1}, \mathbf{q}_1^{l+1}, \mathbf{q}_2, \boldsymbol{\kappa}_1^l, \boldsymbol{\kappa}_2^l) \\ & \text{s.t. } \mathbf{C}\mathbf{q}_2 = \mathbf{1}_K, \end{aligned} \tag{22}$$

3: Update $\rho^{l+1}, \boldsymbol{\kappa}_1^{l+1}, \boldsymbol{\kappa}_2^{l+1}$ by

$$\rho^{l+1} = \begin{cases} \delta \rho^l, & \text{if } \|\mathbf{p}^{l+1} - \mathbf{p}^l\| = 0, \\ \rho^l, & \text{else,} \end{cases} \tag{23}$$

$$\boldsymbol{\kappa}_1^{l+1} := \boldsymbol{\kappa}_1^l + \rho^{l+1}(\mathbf{q}_1^{l+1} - \mathbf{p}^{l+1}), \tag{24}$$

$$\boldsymbol{\kappa}_2^{l+1} := \boldsymbol{\kappa}_2^l + \rho^{l+1}(\mathbf{q}_2^{l+1} - \mathbf{p}^{l+1}); \tag{25}$$

4: If $\Lambda^{l+1} = \|\mathbf{q}_1^{l+1} - \mathbf{p}^{l+1}\|^2 + \|\mathbf{q}_2^{l+1} - \mathbf{p}^{l+1}\|^2 < \eta_1$, output $\mathbf{p}^* = \mathbf{p}^{l+1}$. Otherwise, $l := l + 1$, and return to Step 2.

2.4.1 Update of \mathbf{p}^{l+1}

Ignoring the constant terms, Eq. (20) can be rewritten as

$$\begin{aligned} & \min_{\mathbf{p}} f_1(\mathbf{p}) \\ & \text{s.t. } p_i \in \{0, 1\}, i = 1, \dots, K^2, \end{aligned} \tag{26}$$

where $f_1(\mathbf{p}) = \rho^l \mathbf{p}^T \mathbf{p} - \mathbf{g}_2^{lT} \mathbf{p} = \sum_{i=1}^{K^2} (\rho^l p_i^2 - g_{2,i}^l p_i)$ with $\mathbf{g}_2^l = \mathbf{g} + \rho^l(\mathbf{q}_1^l + \mathbf{q}_2^l) + \boldsymbol{\kappa}_1^l + \boldsymbol{\kappa}_2^l$. Note that both the objective function and constraints are independent with respect to p_i . Hence, the solution to (26) is given by

$$p_i = \begin{cases} 0, & \text{if } \tilde{p}_i \leq 0.5, \\ 1, & \text{else,} \end{cases} \tag{27}$$

with $\tilde{\mathbf{p}} = \mathbf{g}_2^l / (2\rho^l)$.

2.4.2 Updates of \mathbf{q}_1^{l+1} and \mathbf{q}_2^{l+1}

Eq. (21) can be recast as

$$\begin{aligned} \min_{\mathbf{q}_1} & \left\| \mathbf{q}_1 - \mathbf{p}^{l+1} + \frac{\boldsymbol{\kappa}_1^l}{\rho^l} \right\|^2 \\ \text{s.t.} & \mathbf{B}\mathbf{q}_1 = \mathbf{1}_K. \end{aligned} \quad (28)$$

The augmented Lagrangian for Problem (28) can be constructed as

$$L_1(\mathbf{q}_1, \mathbf{v}_1) = \left\| \mathbf{q}_1 - \mathbf{p}^{l+1} + \frac{\boldsymbol{\kappa}_1^l}{\rho^l} \right\|^2 + \mathbf{v}_1^T (\mathbf{B}\mathbf{q}_1 - \mathbf{1}_K).$$

Then set the Lagrangian equations, namely, the partial differentiation of $L_1(\mathbf{q}_1, \mathbf{v}_1)$ w.r.t. \mathbf{q}_1 and \mathbf{v}_1 , respectively, to 0, which can be given by

$$2 \left(\mathbf{q}_1 - \mathbf{p}^{l+1} + \frac{\boldsymbol{\kappa}_1^l}{\rho^l} \right) + \mathbf{B}^T \mathbf{v}_1 = 0, \quad (29)$$

$$\mathbf{B}\mathbf{q}_1 = \mathbf{1}_K. \quad (30)$$

We can derive from (29) that

$$\mathbf{q}_1 = \mathbf{p}^{l+1} - \frac{\boldsymbol{\kappa}_1^l}{\rho^l} - \mathbf{B}^T \mathbf{v}_1 / 2. \quad (31)$$

Substituting (31) back into (30), it follows that

$$\mathbf{v}_1 = 2(\mathbf{B}\mathbf{B}^T)^{-1} \left[\mathbf{B} \left(\mathbf{p}^{l+1} - \frac{\boldsymbol{\kappa}_1^l}{\rho^l} \right) - \mathbf{1}_K \right]. \quad (32)$$

Since $\mathbf{B}\mathbf{B}^T = (\mathbf{1}_K^T \otimes \mathbf{I}_K)(\mathbf{1}_K \otimes \mathbf{I}_K) = (\mathbf{1}_K^T \mathbf{1}_K) \otimes \mathbf{I}_K = K\mathbf{I}_K$, \mathbf{v}_1 can be recast as

$$\mathbf{v}_1 = \frac{2}{K} \left[\mathbf{B} \left(\mathbf{p}^{l+1} - \frac{\boldsymbol{\kappa}_1^l}{\rho^l} \right) - \mathbf{1}_K \right]. \quad (33)$$

Substituting (33) back into (31), the closed form solution to (28) can be derived after some algebraic manipulations as

$$\mathbf{q}_1^{l+1} = \mathbf{p}^{l+1} - \frac{\boldsymbol{\kappa}_1^l}{\rho^l} + \mathbf{B}^T \left(\mathbf{1}_K + \frac{\mathbf{B}\boldsymbol{\kappa}_1^l}{\rho^l} - \mathbf{B}\mathbf{p}^{l+1} \right) / K. \quad (34)$$

On the other hand, Eq. (22) can be recast as

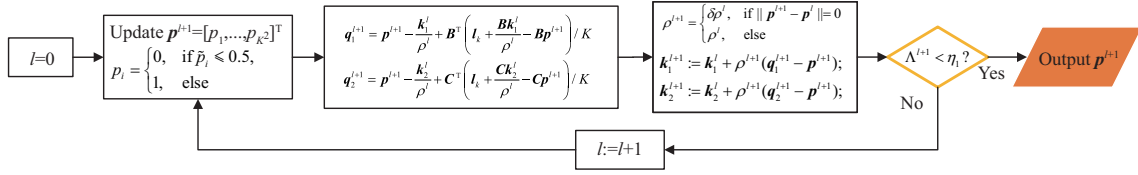
$$\begin{aligned} \min_{\mathbf{q}_2} & \left\| \mathbf{q}_2 - \mathbf{p}^{l+1} + \frac{\boldsymbol{\kappa}_2^l}{\rho^l} \right\|^2 \\ \text{s.t.} & \mathbf{C}\mathbf{q}_2 = \mathbf{1}_K. \end{aligned} \quad (35)$$

Similar to the solving process of (28) with $\mathbf{C}\mathbf{C}^T = K\mathbf{I}_K$, the solution to Problem (35) is

$$\mathbf{q}_2^{l+1} = \mathbf{p}^{l+1} - \frac{\boldsymbol{\kappa}_2^l}{\rho^l} + \mathbf{C}^T \left(\mathbf{1}_K + \frac{\mathbf{C}\boldsymbol{\kappa}_2^l}{\rho^l} - \mathbf{C}\mathbf{p}^{l+1} \right) / K. \quad (36)$$

2.4.3 Computational complexity

Figure 3 shows the flow diagram of Algorithm 1 whose main computational complexity is related to the number of iterations and the size of \mathbf{P} . In each iteration, it costs $O(K^2)$ to compute $\tilde{\mathbf{p}}$ and update $\boldsymbol{\kappa}_1^{l+1}, \boldsymbol{\kappa}_2^{l+1}$, $O(K^3)$ to update \mathbf{q}_1^{l+1} and \mathbf{q}_2^{l+1} . Hence, the total computational complexity in each iteration is $O(K^3)$.


Figure 3 (Color online) Flow diagram of Algorithm 1.

3 Beampattern weight vector synthesis

Considering both the radar and communication performance, we formulate the optimization problem taking into account the MIMO radar beampattern with codebook constraints for both communication cooperative users and eavesdroppers. To solve the resulting optimization problem, an iterative algorithm is developed to get an optimized weight matrix leveraging the ADMM paradigm [42].

3.1 Problem formulation

All possible azimuth angles are divided into several discrete grid sets including the mainlobe $\Omega_{\text{main}} = \{\theta_i\}_{i=1}^I$, sidelobe $\Omega_{\text{side}} = \{\vartheta_s\}_{s=1}^S$, transition regions Φ , directions of UEs $\Omega_{\text{com}} = \{\theta_c^{\text{com}}\}_{c=1}^C$, and directions of eavesdropper $\Omega_{\text{eav}} = \{\theta_h^{\text{eav}}\}_{h=1}^E$, respectively.

To ensure a good MIMO radar beampattern performance, let us consider the transmit beampattern peak mainlobe to sidelobe level ratio (PMSR) as the figure of merit, which is defined as [42]

$$J(\mathbf{w}) = \frac{\min_{\theta_i \in \Omega_{\text{main}}} \|\mathbf{A}^\dagger(\theta_i)\mathbf{w}\|^2}{\max_{\vartheta_s \in \Omega_{\text{side}}} \|\mathbf{A}^\dagger(\vartheta_s)\mathbf{w}\|^2}. \quad (37)$$

Finally, the beampattern design problem for dual-function MIMO radar with codebook constraints specified in (13) and (14) can be expressed as

$$\mathcal{P}_0 \begin{cases} \max_{\mathbf{w}, r_h, b_c \in \mathbb{R}} \log(J(\mathbf{w})) \\ \text{s.t.} & \mathbf{A}^\dagger(\theta_c^{\text{com}})\mathbf{w} = b_c \bar{\mathbf{a}}_1, \quad c = 1, \dots, C, \\ & \mathbf{A}^\dagger(\theta_h^{\text{eav}})\mathbf{w} = r_h \mathbf{1}_K, \quad h = 1, \dots, E, \end{cases}$$

where the log function is to the benefit of processing the fractional objective function afterwards [42]. Note that once the optimal solution \mathbf{w} to \mathcal{P}_0 is obtained, it can be further normalized to the supposed energy by $\mathbf{w}^* = \sqrt{\Delta} \mathbf{w} / \|\mathbf{w}\|$.

Aiming at beampattern peak sidelobe suppressing with symbol phase controlled, \mathcal{P}_0 is a general NP-hard optimization problem due to the non-convexity. In Subsection 3.2, a beampattern optimization with codebook phase controlled (BOC) algorithm leveraging ADMM framework is introduced to get a high quality solution to \mathcal{P}_0 .

3.2 BOC algorithm

By introducing auxiliary variables η , ϵ , \mathbf{y}_i , \mathbf{z}_s , \mathbf{x}_c , and \mathbf{v}_h , \mathcal{P}_0 can be equivalently transformed as [42]

$$\mathcal{P}_1 \begin{cases} \min_{\mathbf{w}, r_h, b_c \in \mathbb{R}} & -\log \frac{\epsilon}{\eta} \\ \mathbf{y}_i, \mathbf{z}_s, \epsilon, \eta & \\ \text{s.t.} & \mathbf{y}_i = \mathbf{A}^\dagger(\theta_i)\mathbf{w}, \quad \|\mathbf{y}_i\|^2 \geq \epsilon, \quad \theta_i \in \Omega_{\text{main}}, \\ & \mathbf{z}_s = \mathbf{A}^\dagger(\vartheta_s)\mathbf{w}, \quad \|\mathbf{z}_s\|^2 \leq \eta, \quad \vartheta_s \in \Omega_{\text{side}}, \\ & \mathbf{x}_c = \mathbf{A}^\dagger(\theta_c^{\text{com}})\mathbf{w}, \quad \mathbf{x}_c = b_c \bar{\mathbf{a}}_1, \quad c = 1, \dots, C, \\ & \mathbf{v}_h = \mathbf{A}^\dagger(\theta_h^{\text{eav}})\mathbf{w}, \quad \mathbf{v}_h = r_h \mathbf{1}_K, \quad h = 1, \dots, E. \end{cases}$$

Therefore, the augmented Lagrangian is defined as

$$\begin{aligned}
 L_{\rho}(\mathbf{w}, \mathbf{y}_i, \epsilon, \mathbf{z}_s, \eta, \mathbf{x}_c, \mathbf{v}_h, \boldsymbol{\mu}_i, \boldsymbol{\nu}_s, \boldsymbol{\xi}_c, \boldsymbol{\lambda}_h) = & -\log \frac{\epsilon}{\eta} + \frac{\rho_1}{2} \sum_{i=1}^I \left(\left\| \mathbf{y}_i - \mathbf{A}^{\dagger}(\theta_i) \mathbf{w} + \boldsymbol{\mu}_i \right\|^2 - \|\boldsymbol{\mu}_i\|^2 \right) \\
 & + \frac{\rho_1}{2} \sum_{s=1}^S \left(\left\| \mathbf{z}_s - \mathbf{A}^{\dagger}(\vartheta_s) \mathbf{w} + \boldsymbol{\nu}_s \right\|^2 - \|\boldsymbol{\nu}_s\|^2 \right) + \frac{\rho_2}{2} \sum_{c=1}^C \left(\left\| \mathbf{x}_c - \mathbf{A}^{\dagger}(\theta_c^{\text{com}}) \mathbf{w} + \boldsymbol{\xi}_c \right\|^2 - \|\boldsymbol{\xi}_c\|^2 \right) \\
 & + \frac{\rho_3}{2} \sum_{h=1}^E \left(\left\| \mathbf{v}_h - \mathbf{A}^{\dagger}(\theta_h^{\text{eav}}) \mathbf{w} + \boldsymbol{\lambda}_h \right\|^2 - \|\boldsymbol{\lambda}_h\|^2 \right),
 \end{aligned}$$

where $\boldsymbol{\rho} = [\rho_1, \rho_2, \rho_3]^T$ is the penalty weight vector, and $\boldsymbol{\mu}_i, \boldsymbol{\nu}_s, \boldsymbol{\xi}_c, \boldsymbol{\lambda}_h$ are the scaled dual variables.

In the following, the ADMM algorithm is employed to determine $\mathbf{w}, \mathbf{y}_i, \epsilon, \mathbf{z}_s, \eta, \mathbf{x}_c, \mathbf{v}_h, \boldsymbol{\mu}_i, \boldsymbol{\nu}_s, \boldsymbol{\xi}_c, \boldsymbol{\lambda}_h$ in an alternating iterative fashion accounting for the constraints in Problem \mathcal{P}_1 . In particular, letting $\mathbf{w}^{(t)}, \{\mathbf{y}_i^{(t)}\}, \epsilon^{(t)}, \{\mathbf{z}_s^{(t)}\}, \eta^{(t)}, \{\mathbf{x}_c^{(t)}\}, \{\mathbf{v}_h^{(t)}\}, \{\boldsymbol{\mu}_i^{(t)}\}, \{\boldsymbol{\nu}_s^{(t)}\}, \{\boldsymbol{\xi}_c^{(t)}\}, \{\boldsymbol{\lambda}_h^{(t)}\}$ denote the t -th iteration values of $\mathbf{w}, \mathbf{y}_i, \epsilon, \mathbf{z}_s, \eta, \mathbf{x}_c, \mathbf{v}_h, \boldsymbol{\mu}_i, \boldsymbol{\nu}_s, \boldsymbol{\xi}_c, \boldsymbol{\lambda}_h$, the procedure of BOC algorithm is reported in Algorithm 2.

Remark 1. Note that if there is no eavesdropper, we can solve the simplified \mathcal{P}_0 without the constraint (14) with the same line of reasoning of Algorithm 2 by setting $\rho_3 = 0$ and neglecting the solving procedure of (42) and (46).

Algorithm 2 BOC algorithm for \mathcal{P}_1

Require: $\{\mathbf{y}_i^{(0)}\}, \epsilon^{(0)}, \{\mathbf{z}_s^{(0)}\}, \eta^{(0)}, \{\mathbf{x}_c^{(0)}\}, \{\mathbf{v}_h^{(0)}\}, \{\boldsymbol{\mu}_i^{(0)}\}, \{\boldsymbol{\nu}_s^{(0)}\}, \{\boldsymbol{\xi}_c^{(0)}\}, \{\boldsymbol{\lambda}_h^{(0)}\}, \boldsymbol{\rho}, \Delta, \eta_2$;

Ensure: MIMO radar weight vector \mathbf{w}^* ;

1: $t = 0$;

2: Update $\mathbf{w}^{(t)}, \{\mathbf{y}_i^{(t)}\}, \epsilon^{(t)}, \{\mathbf{z}_s^{(t)}\}, \eta^{(t)}, \{\mathbf{x}_c^{(t)}\}, \{\mathbf{v}_h^{(t)}\}$ by solving the following problems:

$$\mathbf{w}^{(t+1)} := \arg \min_{\mathbf{w}} L_{\rho}(\mathbf{w}, \{\mathbf{y}_i^{(t)}\}, \epsilon^{(t)}, \{\mathbf{z}_s^{(t)}\}, \eta^{(t)}, \{\mathbf{x}_c^{(t)}\}, \{\mathbf{v}_h^{(t)}\}, \{\boldsymbol{\mu}_i^{(t)}\}, \{\boldsymbol{\nu}_s^{(t)}\}, \{\boldsymbol{\xi}_c^{(t)}\}, \boldsymbol{\lambda}_h^{(t)}); \quad (38)$$

$$\begin{aligned}
 \{\mathbf{y}_i^{(t+1)}, \epsilon^{(t+1)}\} &:= \arg \min_{\mathbf{y}_i, \epsilon} L_{\rho}(\mathbf{w}^{(t+1)}, \{\mathbf{y}_i\}, \epsilon, \{\mathbf{z}_s^{(t)}\}, \eta^{(t)}, \{\mathbf{x}_c^{(t)}\}, \{\mathbf{v}_h^{(t)}\}, \{\boldsymbol{\mu}_i^{(t)}\}, \{\boldsymbol{\nu}_s^{(t)}\}, \{\boldsymbol{\xi}_c^{(t)}\}, \boldsymbol{\lambda}_h^{(t)}) \\
 \text{s.t. } &\|\mathbf{y}_i\|^2 \geq \epsilon, \quad i = 1, \dots, I;
 \end{aligned} \quad (39)$$

$$\begin{aligned}
 \{\mathbf{z}_s^{(t+1)}, \eta^{(t+1)}\} &:= \arg \min_{\mathbf{z}_s, \eta} L_{\rho}(\mathbf{w}^{(t+1)}, \{\mathbf{y}_i^{(t+1)}\}, \epsilon^{(t+1)}, \{\mathbf{z}_s\}, \eta, \{\mathbf{x}_c^{(t)}\}, \{\mathbf{v}_h^{(t)}\}, \{\boldsymbol{\mu}_i^{(t)}\}, \{\boldsymbol{\nu}_s^{(t)}\}, \{\boldsymbol{\xi}_c^{(t)}\}, \boldsymbol{\lambda}_h^{(t)}) \\
 \text{s.t. } &\|\mathbf{z}_s\|^2 \leq \eta, \quad s = 1, \dots, S;
 \end{aligned} \quad (40)$$

$$\begin{aligned}
 \{\mathbf{x}_c^{(t+1)}, b_c^{(t+1)}\} &:= \arg \min_{\mathbf{x}_c, b_c \in \mathbb{R}} L_{\rho}(\mathbf{w}^{(t+1)}, \{\mathbf{y}_i^{(t+1)}\}, \epsilon^{(t+1)}, \{\mathbf{z}_s^{(t+1)}\}, \eta^{(t+1)}, \{\mathbf{x}_c\}, \{\mathbf{v}_h^{(t)}\}, \{\boldsymbol{\mu}_i^{(t)}\}, \{\boldsymbol{\nu}_s^{(t)}\}, \{\boldsymbol{\xi}_c^{(t)}\}, \boldsymbol{\lambda}_h^{(t)}) \\
 \text{s.t. } &\mathbf{x}_c = b_c \bar{\mathbf{a}}_1, \quad c = 1, \dots, C;
 \end{aligned} \quad (41)$$

$$\begin{aligned}
 \{\mathbf{v}_h^{(t+1)}, r_h^{(t+1)}\} &:= \arg \min_{\mathbf{v}_h, r_h} L_{\rho}(\mathbf{w}^{(t+1)}, \{\mathbf{y}_i^{(t+1)}\}, \epsilon^{(t+1)}, \{\mathbf{z}_s^{(t+1)}\}, \eta^{(t+1)}, \{\mathbf{x}_c^{(t+1)}\}, \{\mathbf{v}_h\}, \{\boldsymbol{\mu}_i^{(t)}\}, \{\boldsymbol{\nu}_s^{(t)}\}, \{\boldsymbol{\xi}_c^{(t)}\}, \boldsymbol{\lambda}_h^{(t)}) \\
 \text{s.t. } &\mathbf{v}_h = r_h \mathbf{1}_K, \quad h = 1, \dots, E.
 \end{aligned} \quad (42)$$

3: Update $\{\boldsymbol{\mu}_i^{(t+1)}\}, \{\boldsymbol{\nu}_s^{(t+1)}\}, \{\boldsymbol{\xi}_c^{(t+1)}\}, \{\boldsymbol{\lambda}_h^{(t+1)}\}$ by

$$\boldsymbol{\mu}_i^{(t+1)} := \boldsymbol{\mu}_i^{(t)} + \mathbf{y}_i^{(t+1)} - \mathbf{A}^{\dagger}(\theta_i) \mathbf{w}^{(t+1)}; \quad (43)$$

$$\boldsymbol{\nu}_s^{(t+1)} := \boldsymbol{\nu}_s^{(t)} + \mathbf{z}_s^{(t+1)} - \mathbf{A}^{\dagger}(\vartheta_s) \mathbf{w}^{(t+1)}; \quad (44)$$

$$\boldsymbol{\xi}_c^{(t+1)} := \boldsymbol{\xi}_c^{(t)} + \mathbf{x}_c^{(t+1)} - \mathbf{A}^{\dagger}(\theta_c^{\text{com}}) \mathbf{w}^{(t+1)}; \quad (45)$$

$$\boldsymbol{\lambda}_h^{(t+1)} := \boldsymbol{\lambda}_h^{(t)} + \mathbf{v}_h^{(t+1)} - \mathbf{A}^{\dagger}(\theta_h^{\text{eav}}) \mathbf{w}^{(t+1)}; \quad (46)$$

4: If $\Theta^{(t+1)} = \sum_{i=1}^I \|\mathbf{y}_i^{(t+1)} - \mathbf{A}^{\dagger}(\theta_i) \mathbf{w}^{(t+1)}\|^2 + \sum_{s=1}^S \|\mathbf{z}_s^{(t+1)} - \mathbf{A}^{\dagger}(\vartheta_s) \mathbf{w}^{(t+1)}\|^2 + \sum_{c=1}^C \|\mathbf{x}_c^{(t+1)} - \mathbf{A}^{\dagger}(\theta_c^{\text{com}}) \mathbf{w}^{(t+1)}\|^2 + \sum_{h=1}^E \|\mathbf{v}_h^{(t+1)} - \mathbf{A}^{\dagger}(\theta_h^{\text{eav}}) \mathbf{w}^{(t+1)}\|^2 < \eta_2$, output $\mathbf{w}^* = \sqrt{\Delta} \mathbf{w}^{(t+1)} / \|\mathbf{w}^{(t+1)}\|$ with the supposed energy Δ . Otherwise, $t := t + 1$, and return to Step 2.

3.2.1 Update of $\mathbf{w}^{(t+1)}$

Eq. (38) can be equivalently recast as

$$\min_{\mathbf{w}} \mathbf{w}^{\dagger} \mathbf{R} \mathbf{w} - \Re\{\mathbf{d}^{\dagger} \mathbf{w}\}, \quad (47)$$

where

$$\mathbf{R} = \frac{1}{2} \sum_{\phi \in \Omega} \rho(\phi) \mathbf{A}(\phi) \mathbf{A}^\dagger(\phi), \quad (48)$$

$$\mathbf{d} = \sum_{\phi \in \Omega} \rho(\phi) \mathbf{A}(\phi) \mathbf{u}(\phi), \quad (49)$$

$$\rho(\phi) = \begin{cases} \rho_1, & \phi \in \Omega_{\text{main}} \cup \Omega_{\text{side}}, \\ \rho_2, & \phi \in \Omega_{\text{com}}, \\ \rho_3, & \phi \in \Omega_{\text{eav}}, \end{cases} \quad (50)$$

$$\mathbf{u}(\phi) = \begin{cases} \mathbf{y}_i + \boldsymbol{\mu}_i, & \text{if } \phi = \theta_i, \theta_i \in \Omega_{\text{main}}, \\ \mathbf{z}_s + \boldsymbol{\nu}_s, & \text{if } \phi = \vartheta_s, \vartheta_s \in \Omega_{\text{side}}, \\ \mathbf{x}_c + \boldsymbol{\xi}_s, & \text{if } \phi = \theta_c^{\text{com}}, \theta_c^{\text{com}} \in \Omega_{\text{com}}, \\ \mathbf{v}_h + \boldsymbol{\lambda}_h, & \text{if } \phi = \theta_h^{\text{eav}}, \theta_h^{\text{eav}} \in \Omega_{\text{eav}}, \end{cases} \quad (51)$$

with $\Omega = \Omega_{\text{main}} \cup \Omega_{\text{side}} \cup \Omega_{\text{com}} \cup \Omega_{\text{eav}}$.

As a consequence, its closed form solution can be readily derived as

$$\mathbf{w}^{(t+1)} = \mathbf{R}^{-1} \mathbf{d} / 2. \quad (52)$$

3.2.2 Updates of $\{\mathbf{y}_i^{(t+1)}\}, \epsilon^{(t+1)}, \{\mathbf{z}_s^{(t+1)}\}, \eta^{(t+1)}$

Ignoring the irrelevant constant terms, Problems (39) and (40) can be equivalently transformed to

$$\begin{aligned} \min_{\mathbf{y}_i, \epsilon} & -\log \epsilon + \frac{\rho_1}{2} \sum_{i=1}^I \|\mathbf{y}_i - \bar{\mathbf{y}}_i^{(t)}\|^2 \\ \text{s.t.} & \|\mathbf{y}_i\|^2 \geq \epsilon, \quad i = 1, \dots, I, \end{aligned} \quad (53)$$

and

$$\begin{aligned} \min_{\mathbf{z}_s, \eta} & \log \eta + \frac{\rho_1}{2} \sum_{s=1}^S \|\mathbf{z}_s - \bar{\mathbf{z}}_s^{(t)}\|^2 \\ \text{s.t.} & \|\mathbf{z}_s\|^2 \leq \eta, \quad s = 1, \dots, S, \end{aligned} \quad (54)$$

respectively, with $\bar{\mathbf{y}}_i^{(t)} = \mathbf{A}^\dagger(\theta_i) \mathbf{w}^{(t+1)} - \boldsymbol{\mu}_i^{(t)}$ and $\bar{\mathbf{z}}_s^{(t)} = \mathbf{A}^\dagger(\vartheta_s) \mathbf{w}^{(t+1)} - \boldsymbol{\nu}_s^{(t)}$.

Let us first focus on Problem (53). Specifically, once $\epsilon^{(t+1)}$ is obtained, $\{\mathbf{y}_i^{(t+1)}\}$ can be derived as the scaled version of $\bar{\mathbf{y}}_i^{(t)}$, given by

$$\mathbf{y}_i^{(t+1)} = \begin{cases} \bar{\mathbf{y}}_i^{(t)}, & \text{if } \|\bar{\mathbf{y}}_i^{(t)}\|^2 > \epsilon^{(t+1)}, \\ \sqrt{\epsilon^{(t+1)}} \frac{\bar{\mathbf{y}}_i^{(t)}}{\|\bar{\mathbf{y}}_i^{(t)}\|}, & \text{otherwise.} \end{cases} \quad (55)$$

Then, another optimization problem with respect to ϵ can be obtained by substituting (55) back into (53):

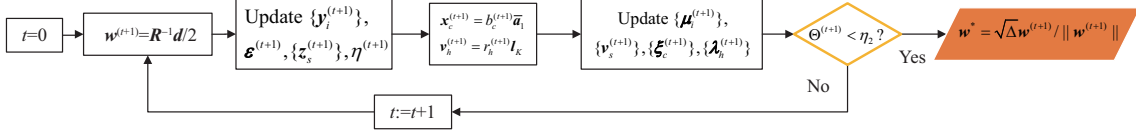
$$\min_{\epsilon} f_1(\epsilon), \quad (56)$$

where

$$f_1(\epsilon) = -\log(\epsilon) + \frac{\rho_1}{2} \sum_{i=1}^I \hat{\omega}_i \left(\sqrt{\epsilon} - \|\bar{\mathbf{y}}_i^{(t)}\| \right)^2, \quad (57)$$

$$\hat{\omega}_i = \begin{cases} 0, & \text{if } \|\bar{\mathbf{y}}_i^{(t)}\|^2 > \epsilon, \\ 1, & \text{otherwise.} \end{cases} \quad (58)$$

Similarly, given $\eta^{(t+1)}$, $\{\mathbf{z}_s^{(t+1)}\}$ is the scaled version of $\bar{\mathbf{z}}_s^{(t)}$, i.e.,


Figure 4 (Color online) Flow diagram of Algorithm 2.

$$\mathbf{z}_s^{(t+1)} = \begin{cases} \sqrt{\eta^{(t+1)}} \frac{\bar{\mathbf{z}}_s^{(t)}}{\|\bar{\mathbf{z}}_s^{(t)}\|}, & \text{if } \|\bar{\mathbf{z}}_s^{(t)}\|^2 > \eta^{(t+1)}, \\ \bar{\mathbf{z}}_s^{(t)}, & \text{otherwise.} \end{cases} \quad (59)$$

Substituting (59) back into (54) yields

$$\min_{\eta} f_2(\eta), \quad (60)$$

where

$$f_2(\eta) = \log(\eta) + \frac{\rho_1}{2} \sum_{s=1}^S \bar{\omega}_s \left(\sqrt{\eta} - \|\bar{\mathbf{z}}_s^{(t)}\| \right)^2, \quad (61)$$

$$\bar{\omega}_s = \begin{cases} 0, & \text{if } \|\bar{\mathbf{z}}_s^{(t)}\|^2 \leq \eta, \\ 1, & \text{otherwise.} \end{cases} \quad (62)$$

Notice that Problems (56) and (60) have similar structure without constraints, which can be solved by [42] with closed form solutions.

3.2.3 Updates of $\mathbf{x}_c^{(t+1)}$ and $\mathbf{v}_h^{(t+1)}$

Eq. (41) can be recast as

$$\min_{b_c \in \mathbb{R}} \|b_c \bar{\mathbf{a}}_1 - \bar{\mathbf{x}}_c^{(t)}\|^2, \quad (63)$$

where $\bar{\mathbf{x}}_c^{(t)} = \mathbf{A}^\dagger(\theta_c^{\text{com}}) \mathbf{w}^{(t+1)} - \boldsymbol{\xi}_c^{(t)}$. Observing that the objective function is quadratic with respect to b_c , its solution can be easily derived by

$$b_c^{(t+1)} = \frac{\Re\{\bar{\mathbf{a}}_1^\dagger \bar{\mathbf{x}}_c^{(t)}\}}{K}, \quad (64)$$

which follows that $\mathbf{x}_c^{(t+1)} = b_c^{(t+1)} \bar{\mathbf{a}}_1$.

Similarly, Problem (42) can be rewritten as

$$\min_{r_h} \|r_h \mathbf{1}_K - \bar{\mathbf{v}}_h^{(t)}\|^2, \quad (65)$$

where $\bar{\mathbf{v}}_h^{(t)} = \mathbf{A}^\dagger(\theta_h^{\text{eav}}) \mathbf{w}^{(t+1)} - \boldsymbol{\lambda}_h^{(t)}$. Its closed form solution is

$$r_h^{(t+1)} = \frac{\mathbf{1}_K^\top \bar{\mathbf{v}}_h^{(t)}}{K}, \quad (66)$$

which follows that $\mathbf{v}_h^{(t+1)} = r_h^{(t+1)} \mathbf{1}_K$.

3.3 Computational complexity and convergence performance

Let us now analyze the computational complexity of Algorithm 2 whose flow diagram is shown in Figure 4. \mathbf{R}^{-1} and \mathbf{d} can be computed and saved before BOC algorithm starts with a complexity of $O(QM^2 + (KM)^{2.373})$ [42] and $O(QMK)$, respectively, where $Q = I + S + C + E$. In each iteration, Eqs. (38)–(46) are supposed to be solved by simple closed form solutions. Thus, only basic matrix-to-vector multiplications are required. Specifically, the computational complexities of (38), (39)–(42), (43)–(46) are $O(K^2M^2)$, $O(KQ)$, and $O(KMQ)$, respectively. As a consequence, the total computational complexity of Algorithm 2 is $O(QM^2 + (KM)^{2.373} + T_0(K^2M^2 + KMQ))$ with the number of iterations T_0 .

As to the convergence performance of Algorithm 2, the following theorem shows that the sequences generated by the proposed algorithms are convergent under some mild conditions [43].

Theorem 1. Assuming that $\lim_{t \rightarrow \infty} \boldsymbol{\mu}_i^{(t)} - \boldsymbol{\mu}_i^{(t-1)} = \mathbf{0}$, $\lim_{t \rightarrow \infty} \boldsymbol{\nu}_s^{(t)} - \boldsymbol{\nu}_s^{(t-1)} = \mathbf{0}$, $\lim_{t \rightarrow \infty} \boldsymbol{\xi}_c^{(t)} - \boldsymbol{\xi}_c^{(t-1)} = \mathbf{0}$, $\lim_{t \rightarrow \infty} \boldsymbol{\lambda}_h^{(t)} - \boldsymbol{\lambda}_h^{(t-1)} = \mathbf{0}$, a limit point $\{\boldsymbol{w}^*, \boldsymbol{y}_i^*, \boldsymbol{\epsilon}^*, \boldsymbol{z}_s^*, \boldsymbol{\eta}^*, \boldsymbol{x}_c^*, \boldsymbol{v}_h^*, \boldsymbol{\mu}_i^*, \boldsymbol{\nu}_s^*, \boldsymbol{\xi}_c^*, \boldsymbol{\lambda}_h^*\}$ exists, which is a stationary solution to \mathcal{P}_1 .

Proof. See Appendix A for details.

4 Performance analysis

This section is devoted to the performance assessment of the proposed framework in terms of radar beam pattern, constellation diagram, symbol error rate (SER), as well as convergence property. In this respect, an MIMO radar with $M = 10$ transmit elements is considered with spaced half wavelength apart. The spatial angles $\Omega_{\text{main}} = [-15^\circ, 15^\circ]$, $\Phi = [-23^\circ, -16^\circ] \cup [16^\circ, 23^\circ]$, $\Omega_{\text{side}} = [-90^\circ, -24^\circ] \cup [24^\circ, 90^\circ]$ are divided into grids with uniform angle interval 1° .

As to the synthesis of \boldsymbol{w} in Algorithm 2 (named BOC), the exit condition $\eta_2 = K \times 10^{-8}$ is applied with penalty factor $\rho_1 = \rho_2 = 1$, and $\rho_3 = 1$ if $E \geq 1$, $\rho_3 = 0$ if $E = 0$. Scaled dual variables $\{\boldsymbol{\mu}_i^{(0)}\}, \{\boldsymbol{\nu}_s^{(0)}\}, \{\boldsymbol{\xi}_c^{(0)}\}, \{\boldsymbol{\lambda}_h^{(0)}\}$ and auxiliary variables $\{\boldsymbol{y}_i^{(0)}\}, \boldsymbol{\epsilon}^{(0)}, \{\boldsymbol{z}_s^{(0)}\}, \boldsymbol{\eta}^{(0)}, \{\boldsymbol{x}_c^{(0)}\}, \{\boldsymbol{v}_h^{(0)}\}$ are initialized in a random manner. The total transmit energy is set as $\Delta = M$.

4.1 JRC performance with $C = 1$

For comparison purpose, let us consider transmit radiation pattern invariance and selection method [38] (named TRPIS)⁴, as well as variants of the ADMM with linearized approximation (LA) and quadratic approximation (QA) in [45] (named LA-ADMM and QA-ADMM, respectively) and monotonic iterative method for spectrum shaping (MISS) [46] as benchmarks⁵ with the same spatial region division.

Let us first consider one communication receiver (i.e., $C = 1$) located at $\theta_1^{\text{com}} = -14^\circ$ without eavesdropper (i.e., $E = 0$). Figures 5(a)–(c) depict the MIMO radar beam pattern achieved by the proposed BOC algorithm, TRPIS, LA-ADMM, QA-ADMM, and MISS, assuming at the design stage $K = 4, 8, 16$, respectively. Furthermore, Table 1 reports the achieved $J(\boldsymbol{w})$ (in dB) and required time to shed light on corresponding computational complexity. As expected, the larger K , the more running time is required. Moreover, looking over Figures 5(a)–(c) and Table 1 reveals that the proposed BOC algorithm outperforms other counterparts in terms of obtaining a higher PMSR using less running time generally, which provides a practical proof of the BOC framework effectiveness. Comparatively, TRPIS requires to specify the masks on the beam pattern sidelobe, which is hard to ensure the feasibility. MISS which actually involved the majorization-minimization framework, demands for plenty of time due to its large computational complexity. LA-ADMM and QA-ADMM suffer from low PMSR as the integrated sidelobe to mainlobe ratio (ISMR) is minimized without specific consideration on the ripple control.

Corresponding constellation diagrams of $\boldsymbol{s}(\theta_1^{\text{com}})$ (i.e., $|\boldsymbol{s}(\theta_1^{\text{com}})|$ versus $\arg(\boldsymbol{s}(\theta_1^{\text{com}}))$ in polar coordinates) for $K = 4, 8, 16$, are shown in Figures 6(a)–(c), respectively. The amplitudes of $\boldsymbol{s}(\theta_1^{\text{com}})$ decrease versus K generally. Besides, BOC is capable of obtaining a larger amplitude of $\boldsymbol{s}(\theta_1^{\text{com}})$ compared with other counterparts for a given K , which is consistent with $P(\theta_1^{\text{com}})$ shown in Figure 5. Furthermore, $\arg(\boldsymbol{s}(\theta_1^{\text{com}}))$ derived by BOC, LA-ADMM, QA-ADMM, and MISS algorithms are, respectively, uniformly distributed at $2\pi(k-1)/K, k = 1, \dots, K$, whereas that of TRPIS has slight deviations due to its intrinsic complex roots selection scheme.

To shed light on the demodulation performance, 10^4 symbols are randomly generated among K kinds of cases⁶, where an exhaustive search cannot work anymore especially when K is large. As a consequence, the proposed Algorithm 1 is used to demodulate with $\rho^0 = 0.01$, $\eta_1 = 10^{-4}$, and $\delta = 1.01$. Let us first define the power noise ratio (PNR) and signal to noise ratio (SNR) at the c -th receiver end by $\text{PNR} = |\alpha_c|^2 / \sigma_n^2$, and $\text{SNR} = \|\alpha_c \boldsymbol{P}_i^T \boldsymbol{s}(\theta_c^{\text{com}})\|^2 / \sigma_n^2 = P(\theta) \times \text{PNR}$, respectively. The SER of the proposed BOC algorithm, TRPIS, LA-ADMM, QA-ADMM, and MISS for the UE as a function of K versus PNR

4) A principle weight vector with the sidelobes kept below 20 dB is optimized by the minimax criterion, which multiplies with K complex roots to form K weight vectors with the same beam pattern but different angles towards the communication direction [44]. As a result, TRPIS can only deal with one communication receiver and cannot take into account both the beam pattern performance and constellation diagram towards the eavesdroppers' direction.

5) Although LA-ADMM, QA-ADMM, and MISS are not provided in [45, 46] with reference to consistent with constraint (13), their extension to encompass this design constraint is straightforward.

6) The proposed DFRC MIMO scheme communicates with users by embedding information into the permutation matrix \boldsymbol{P} . Hence, the weight matrix is only designed once by Algorithm 2 for a desired radar beam pattern at the beginning.

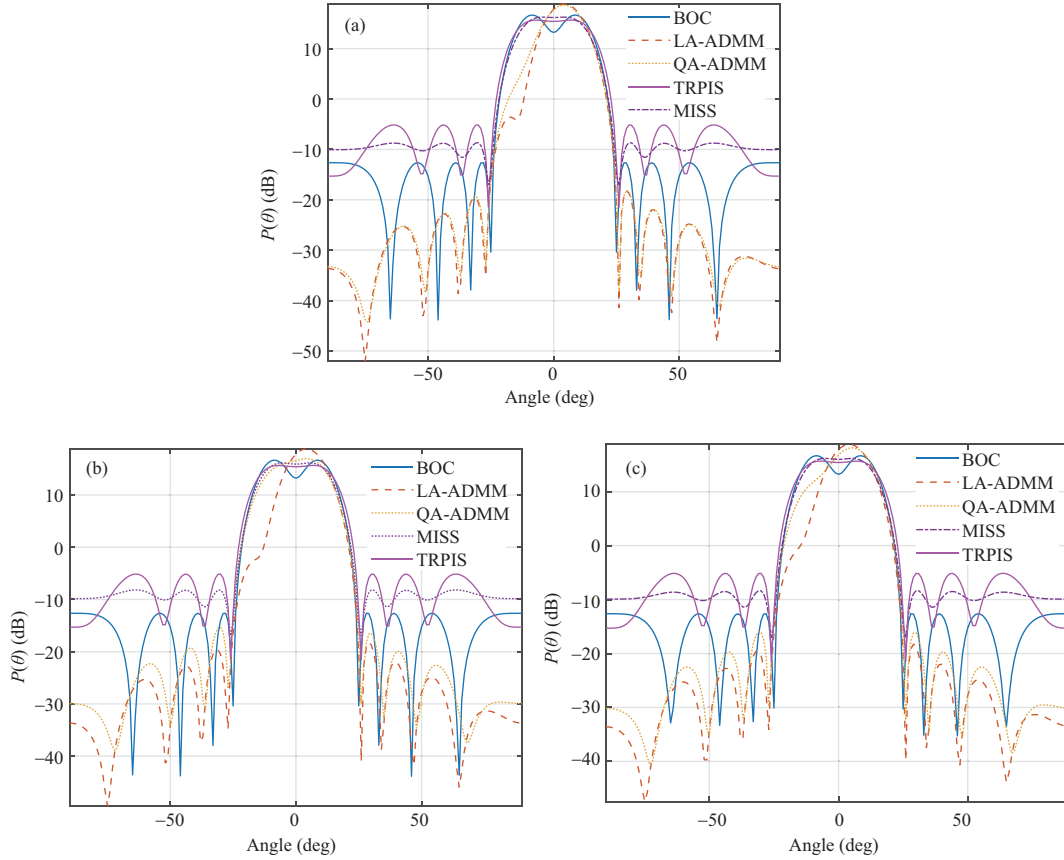


Figure 5 (Color online) Radar beampattern with (a) $K = 4$, (b) $K = 8$, (c) $K = 16$, assuming that $\theta_1^{\text{com}} = -14^\circ$.

Table 1 Achieved $J(\mathbf{w})$ (in dB) and required time for different methods

Method	BOC		TRPIS		LA-ADMM		QA-ADMM		MISS	
	$J(\mathbf{w})$	Time (s)								
$K = 4$	25.869	9.147	18.434	20.934	8.004	285.012	14.797	101.395	20.583	1940.693
$K = 8$	25.868	10.920	18.434	20.994	10.103	412.551	18.918	199.568	20.376	1944.878
$K = 16$	25.854	33.071	18.434	21.242	11.941	1048.964	17.323	619.481	20.480	2030.410

and SNR are shown in Figures 7(a) and (b), respectively. As expected, the increasing of PNR or SNR provides SER improvements. The curves highlight that a lower SER for better demodulation performance can be obtained with a smaller K as a larger minimum distance between constellation points is acquired. Regardless of K , the proposed BOC algorithm outperforms other counterparts in terms of SER with a fixed PNR, since its superiority in higher gain of b_c , whereas the curves of SER versus SNR for a given K almost coincide with each other. In other words, as long as $\arg(\mathbf{s}(\theta_c^{\text{com}}))$ is equally distributed among $[0, 2\pi)$, the demodulation performance depends on the received SNR and K , where SNR further relies on the PNR and $P(\theta)$. Hence, with the same PNR at the receiver end for different synthesized weight matrices, the one which provides higher value of $P(\theta_c^{\text{com}})$, and thus higher SNR, has better demodulation performance. In this respect, we only study the performance of the proposed framework as a typical example in the following.

4.2 JRC performance with $C = 2$

To process further, let us increase one more communication receiver at $\theta_2^{\text{com}} = 40^\circ$ taking the case study of $K = 4$, where Ref. [38] cannot work anymore. Figure 8(a) depicts the radar beampatterns derived by BOC for $C = 2$ receivers by comparisons with that for $\theta_1^{\text{com}} = -14^\circ$ only (i.e., the curve derived by BOC in Figure 5(a)). It shows the beampatterns for different C are similar, while the beampattern with $C = 1$ has deeper notches. Besides, constellation diagrams of $\mathbf{s}(\theta_c^{\text{com}})$, $c = 1, 2$ (i.e., $|\mathbf{s}(\theta_c^{\text{com}})|$ versus $\arg(\mathbf{s}(\theta_c^{\text{com}}))$ in polar coordinates) are shown in Figure 8(b). As expected, the amplitude b_1 is larger than

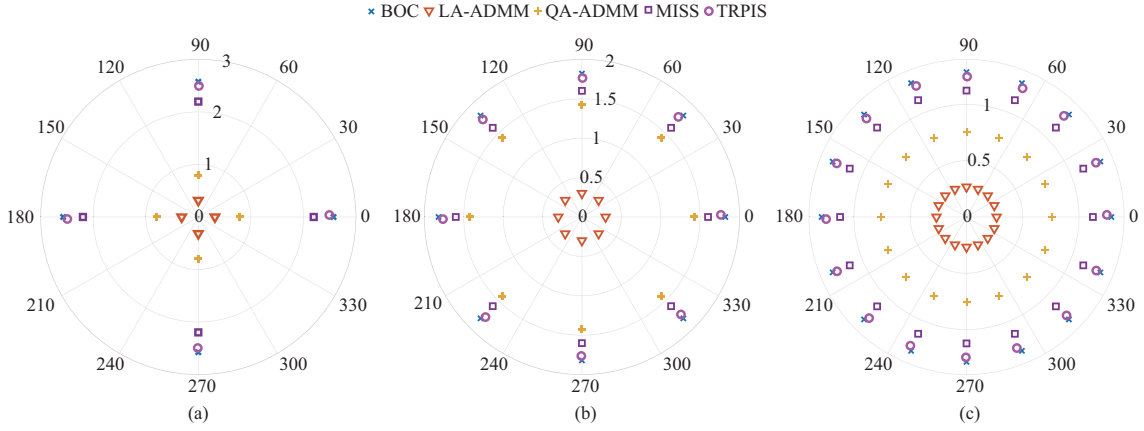


Figure 6 (Color online) Constellation diagram of $s(\theta_1^{\text{com}})$ with (a) $K = 4$, (b) $K = 8$, (c) $K = 16$, assuming that $\theta_1^{\text{com}} = -14^\circ$.

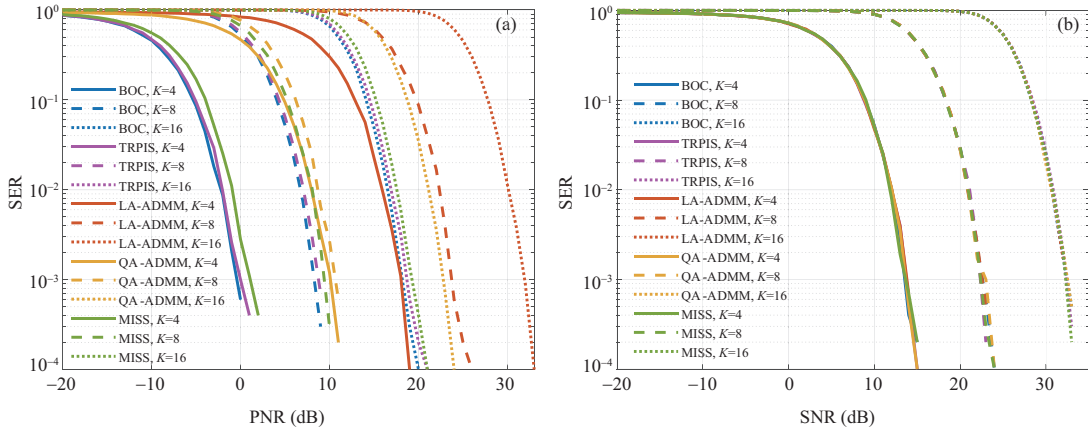


Figure 7 (Color online) SER for different K with $\theta_1^{\text{com}} = -14^\circ$ versus (a) PNR and (b) SNR.

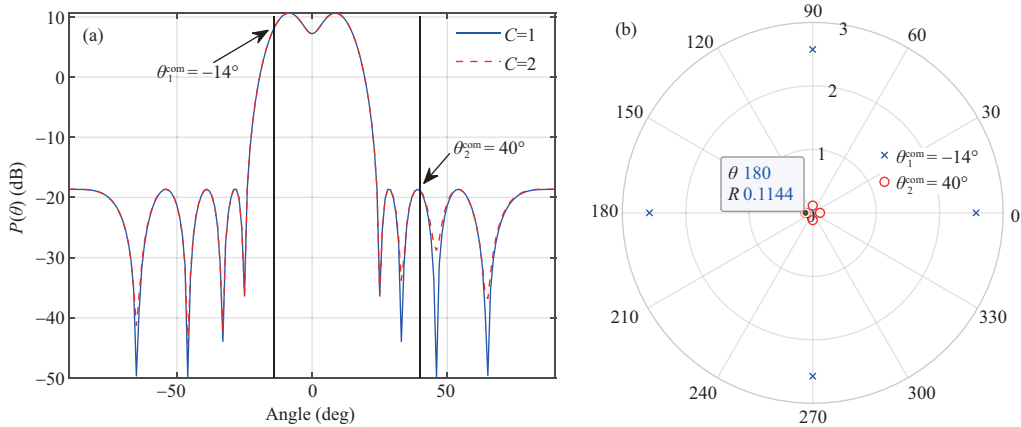


Figure 8 (Color online) DFRC performance of the designed weight vectors for $\theta_1^{\text{com}} = -14^\circ$ and $\theta_2^{\text{com}} = 40^\circ$ with $K = 4$. (a) Radar beampattern; (b) constellation diagram of $s(\theta_c^{\text{com}})$, $c = 1, 2$.

b_2 for $P(\theta_1^{\text{com}}) > P(\theta_2^{\text{com}})$.

Furthermore, SER for θ_c^{com} , $c = 1, 2$, versus PNR and SNR are studied in Figures 9(a) and (b), respectively. As the communication receiver at -14° has higher beampattern gain, the SER of -14° is much lower than that of 40° with the same PNR, which is consistent with Figure 8(b). As expected, Figure 9(b) reveals that the SER versus SNR curves of two communication users are almost coincident, where the compensation of PNR leads to the same amplitude of $a_c b_c$, $c = 1, 2$. The results again verify the demodulation performance with fixed K is only influenced by SNR with a uniformly distributed

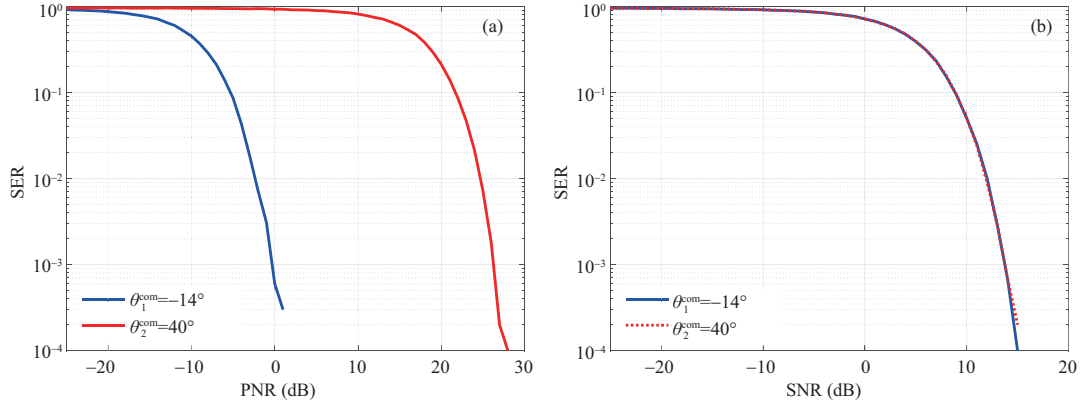


Figure 9 (Color online) SER for $\theta_1^{\text{com}} = -14^\circ$ and $\theta_2^{\text{com}} = 40^\circ$ with $K = 4$ versus (a) PNR and (b) SNR.

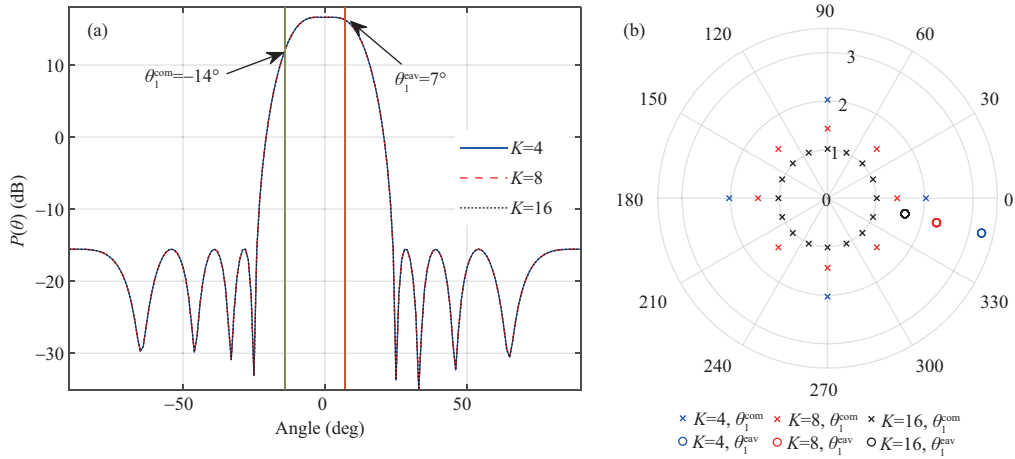


Figure 10 (Color online) DFRC performance of the designed weight vectors for $K = 4, 8, 16$ with $\theta_1^{\text{com}} = -14^\circ$ and $\theta_1^{\text{eav}} = 7^\circ$. (a) MIMO radar beampattern; (b) constellation diagram of $\mathbf{s}(\theta_1^{\text{com}})$ and $\mathbf{s}(\theta_1^{\text{eav}})$.

$\arg(\mathbf{s}(\theta_c^{\text{com}}))$, where SNR is further influenced by PNR and the power radiated to the direction of users.

4.3 JRC performance with $C = 1$ and $E = 1$

To shed light on the performance of preventing eavesdropping, let us assume there are one eavesdropper located at $\theta_1^{\text{eav}} = 7^\circ$ and one communication receiver located at $\theta_1^{\text{com}} = -14^\circ$. In Figures 10(a) and (b), the radar beampattern and the constellation diagram of both $\mathbf{s}(\theta_1^{\text{com}})$ and $\mathbf{s}(\theta_1^{\text{eav}})$ are provided, respectively. The beampatterns in Figure 10(a) are nearly coincident for different K with the PMSR of about 26.58 dB. Furthermore, the entries of $\mathbf{s}(\theta_1^{\text{com}})$ in Figure 10(b) are marked by crosses with $\arg(\mathbf{s}(\theta_c^{\text{com}}))$ uniformly distributed among $[0, 2\pi)$, whereas those of $\mathbf{s}(\theta_1^{\text{eav}})$ marked by circles are totally the same, thus, overlap in the polar coordinates. Inspection of Figure 10 highlights the proposed Algorithm 2 is capable of optimizing the radar beampattern while controlling the symbol phase distribution impinged to both the direction of communication and eavesdropper simultaneously, whereas TRPIS cannot. Figure 11 further depicts the SER versus PNR from the direction of $\theta_1^{\text{com}} = -14^\circ$ for different K . It again reveals that the SER increases versus K for the same PNR as the limited beampattern energy is equally divided into K beams.

To assess the importance of the incorporation of eavesdroppers, let us now compare the demodulation performance of the eavesdropper located at $\theta_1^{\text{eav}} = 7^\circ$ between the tailored design for preventing interception and that derived by BOC with eavesdropper neglected at the design stage in Subsection 4.1. Assuming the modulation mode is precisely known by the eavesdropper, Figure 12 shows SER of the eavesdropper located at $\theta_1^{\text{eav}} = 7^\circ$ associated with the weight vectors synthesized by the proposed Algorithm 2 in Figure 5(a) and in Figure 10(a) for $K = 4$ versus PNR, respectively. Inspection of the plot clearly reveals the effectiveness of preventing interception with a-priori information of the eavesdropper

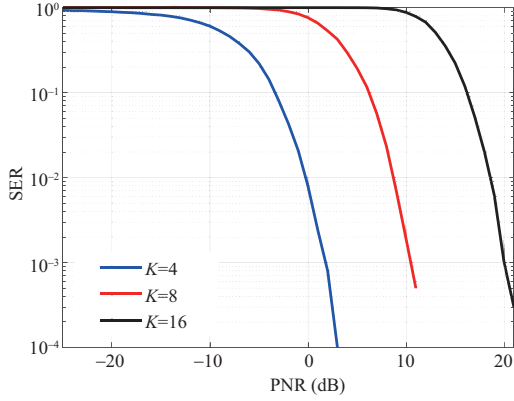


Figure 11 (Color online) SER versus PNR of the UE with $\theta_1^{\text{com}} = -14^\circ$.

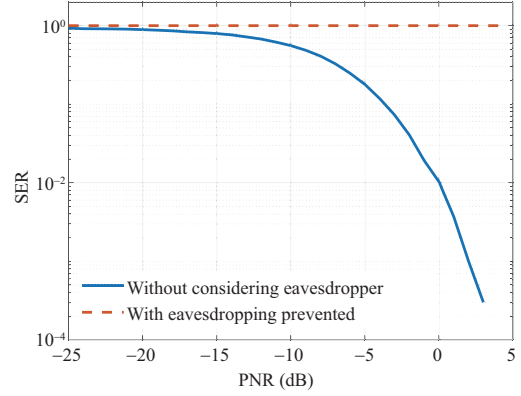


Figure 12 (Color online) SER versus PNR of the eavesdropper with $\theta_1^{\text{eav}} = 7^\circ$.

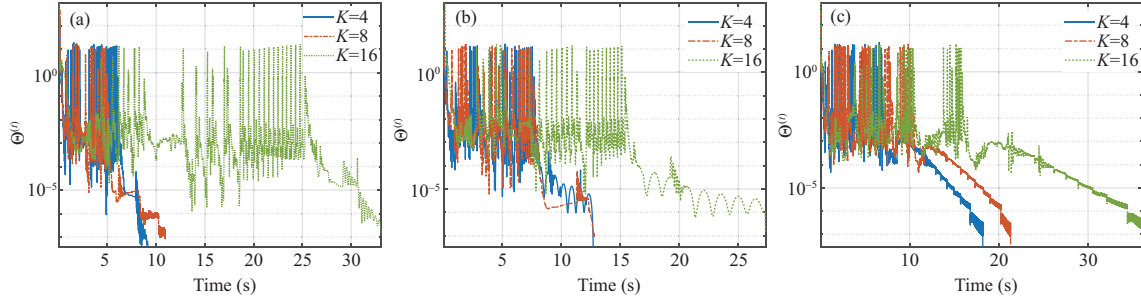


Figure 13 (Color online) $\Theta^{(t)}$ versus time of the proposed Algorithm 2 with the same environmental characterization as (a) in Subsection 4.1 for $C = 1$, (b) in Subsection 4.2 for $C = 2$, (c) in Subsection 4.3 for $C = 1, E = 1$.

considered.

4.4 Computational complexity

To further assess the convergence property and computational complexity of the proposed algorithms, $\Theta^{(t)}$ derived by Algorithm 2 versus time for different K with the same environmental characterization as in Subsections 4.1–4.3 are shown in Figures 13(a)–(c), respectively. Figures 13(a)–(c) indicate the stopping conditions are gradually met for different scenarios and K . Hence, the BOC algorithm converges with constraints satisfied, which is of great importance to accord with the codebook demands for communication and interception prevention. As expected, a larger running time is demanded with increasing K . Moreover, the BOC algorithm converges quickly as a closed-form solution can be obtained in each step of the optimization process, which implies the potential for large-scale optimization.

Figure 14 depicts Λ^l derived by Algorithm 1 with PNR = 0 dB with the same environmental configuration as in Subsection 4.1 as a typical example. Algorithm 1 quickly converges within 0.0248, 0.0341, and 0.2898 s for $K = 4, 8, 16$, respectively, which is applicable for the real-time requirement of demodulation. Furthermore, with l^* denoting the last iteration number before exiting the iteration loop, the convergent parameter $\Lambda^{l^*} = \|\mathbf{q}_1^{l^*} - \mathbf{p}^{l^*}\|^2 + \|\mathbf{q}_2^{l^*} - \mathbf{p}^{l^*}\|^2$ is very close to 0, implying that $\lim_{l \rightarrow \infty} \mathbf{p}^l = \lim_{l \rightarrow \infty} \mathbf{q}_1^l = \lim_{l \rightarrow \infty} \mathbf{q}_2^l$, thus, \mathbf{p}^l converges with permutation matrix constraints satisfied.

5 Conclusion

The DFRC MIMO system with communication information embedded in the permutation matrix has been addressed in this paper, where a series of weight vectors are designed for the desired radar beampattern with codebooks phase control. Specifically, ensuring the phases induced by the designed weight vectors impinged to the directions of the communication receivers and eavesdroppers to be uniformly distributed and totally the same, respectively, the design has aimed at maximizing the PMSR, which formulates a quadratic fractional programming optimization problem with multi-equality constraints. Resorting to the

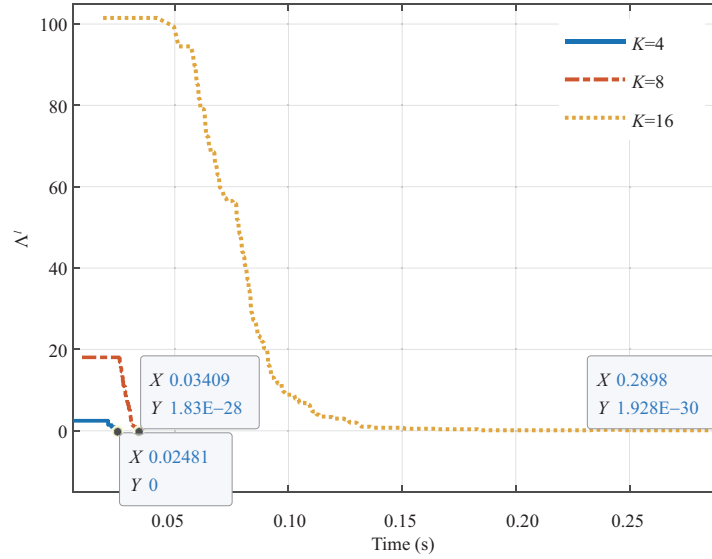


Figure 14 (Color online) A^l versus time of the proposed Algorithm 1 for $K = 4, 8, 16$.

ADMM framework, an iterative procedure named BOC algorithm (with ensured convergence properties under mild conditions) has been proposed. In this respect, convex subproblems can be derived by invoking auxiliary variables in each step, where a global optimal point is obtained in closed form. Remarkably, the overall computational complexity of the proposed BOC algorithm is polynomial with respect to the numbers of transmit antennas and waveform sets of the MIMO radar. Furthermore, to demodulate the information efficiently, the correlation between the communication codebook and permutation of the received filtered data has been considered a figure of merit with the optimized variable supposed to be a permutation matrix. To this end, a novel algorithm based on ADPM has been proposed to tackle the mix-boolean optimization problem, with a computational complexity cubic with reference to the number of waveform sets. At the analysis stage, the performance of the proposed framework has been assessed in terms of radar beampattern, constellation diagram of codebooks, communication performance, and convergence property. Simulation results have clearly revealed that the proposed framework is capable of realizing DFRC for multi-users while preventing interception from eavesdroppers. Besides, some comparisons with counterparts available in the open literature have been provided for the BOC algorithm, showing interesting performance gains, in terms of achieved PMSR and computational time.

Future research tracks might concern the extension of this framework to the wideband MIMO radar [47, 48], FDA-MIMO radar systems where frequency diversity may induce other degrees of freedom to improve the JRC performance [49, 50], as well as the robust design with imperfect channel state information [51].

Acknowledgements This work of Jing YANG, Xianxiang YU, and Guolong CUI was supported in part by National Natural Science Foundation of China (Grant Nos. U19B2017, 62101097, 61871080), Changjiang Scholar Program, 111 Project (Grant No. B17008), and China Postdoctoral Science Foundation (Grant Nos. 2020M680147, 2021T140096).

References

- Zheng L, Lops M, Eldar Y C, et al. Radar and communication coexistence: an overview: a review of recent methods. *IEEE Signal Process Mag*, 2019, 36: 85–99
- Aubry A, de Maio A, Govoni M A, et al. On the design of multi-spectrally constrained constant modulus radar signals. *IEEE Trans Signal Process*, 2020, 68: 2231–2243
- Yang J, Aubry A, de Maio A, et al. Multi-spectrally constrained transceiver design against signal-dependent interference. *IEEE Trans Signal Process*, 2022, 70: 1320–1332
- Aubry A, Carotenuto V, de Maio A, et al. Optimization theory-based radar waveform design for spectrally dense environments. *IEEE Aerosp Electron Syst Mag*, 2016, 31: 14–25
- Yu X, Qiu H, Yang J, et al. Multispectrally constrained MIMO radar beampattern design via sequential convex approximation. *IEEE Trans Aerosp Electron Syst*, 2022, 58: 2935–2949
- Hassanien A, Amin M G, Zhang Y D, et al. Signaling strategies for dual-function radar communications: an overview. *IEEE Aerosp Electron Syst Mag*, 2016, 31: 36–45
- Zhang D, Hu Y, Chen Y, et al. BreathTrack: tracking indoor human breath status via commodity WiFi. *IEEE Int Things J*, 2019, 6: 3899–3911
- Yu X, Yao X, Yang J, et al. Integrated waveform design for MIMO radar and communication via spatio-spectral modulation. *IEEE Trans Signal Process*, 2022, 70: 2293–2305
- Zhu K H, Wang J, Liang X D, et al. Joint SAR imaging and wireless communication using the FBMC chirp waveform. *Sci China Inf Sci*, 2020, 63: 149302

- 10 Bu Y, Qiu H, Fan T, et al. Constant modulus sequence set design with low weighted integrated sidelobe level in spectrally crowded environments. *Sci China Inf Sci*, 2022, 65: 159303
- 11 Yu X, Alhujaili K, Cui G, et al. MIMO radar waveform design in the presence of multiple targets and practical constraints. *IEEE Trans Signal Process*, 2020, 68: 1974–1989
- 12 Cui G, de Maio A, Farina A, et al. *Radar Waveform Design Based on Optimization Theory*. London: SciTech Publishing, 2020
- 13 Yu X, Cui G, Yang J, et al. MIMO radar transmit-receive design for moving target detection in signal-dependent clutter. *IEEE Trans Veh Technol*, 2020, 69: 522–536
- 14 Yao Y, Li X, Wu L. Cognitive frequency-hopping waveform design for dual-function MIMO radar-communications system. *Sensors*, 2020, 20: 415
- 15 Liu Y, Liao G, Chen Y, et al. Super-resolution range and velocity estimations with OFDM integrated radar and communications waveform. *IEEE Trans Veh Technol*, 2020, 69: 11659–11672
- 16 Liu Y, Liao G, Yang Z, et al. Multiobjective optimal waveform design for OFDM integrated radar and communication systems. *Signal Processing*, 2017, 141: 331–342
- 17 Hassanien A, Himed B, Rigling B D. A dual-function MIMO radar-communications system using frequency-hopping waveforms. In: *Proceedings of IEEE Radar Conference*, Seattle, 2017. 1721–1725
- 18 Eedara I P, Amin M G, Hassanien A. Controlling clutter modulation in frequency hopping MIMO dual-function radar communication systems. In: *Proceedings of IEEE International Radar Conference (RADAR)*, Washington, 2020. 466–471
- 19 Eedara I P, Amin M G, Hoorfar A. Optimum code design using genetic algorithm in frequency hopping dual function MIMO radar communication systems. In: *Proceedings of IEEE Radar Conference*, Florence, 2020. 1–6
- 20 Eedara I P, Amin M G, Fabrizio G A. Target detection in frequency hopping MIMO dual-function radar-communication systems. In: *Proceedings of IEEE International Conference on Acoustics, Speech and Signal Processing (ICASSP)*, Toronto, 2021. 8458–8462
- 21 Wang X, Hassanien A. Phase modulated communications embedded in correlated FH-MIMO radar waveforms. In: *Proceedings of IEEE Radar Conference*, Florence, 2020. 1–6
- 22 Wang X, Xu J, Hassanien A, et al. Joint communications with FH-MIMO radar systems: an extended signaling strategy. In: *Proceedings of IEEE International Conference on Acoustics, Speech and Signal Processing (ICASSP)*, Toronto, 2021. 8253–8257
- 23 Sturm C, Wiesbeck W. Waveform design and signal processing aspects for fusion of wireless communications and radar sensing. *Proc IEEE*, 2011, 99: 1236–1259
- 24 Tian X, Song Z. On radar and communication integrated system using OFDM signal. In: *Proceedings of IEEE Radar Conference*, Seattle, 2017. 0318–0323
- 25 Huang Y, Hu S, Ma S, et al. Constant envelope OFDM RadCom fusion system. *J Wireless Com Network*, 2018, 2018: 104
- 26 Ji S, Chen H, Hu Q, et al. A dual-function radar-communication system using FDA. In: *Proceedings of IEEE Radar Conference*, Oklahoma City, 2018. 0224–0229
- 27 Alselwi A, Khan A U, Qureshi I M, et al. Throughput enhancement for the joint radar-communication systems based on cognitive closed-loop design. *IEEE Access*, 2021, 9: 64785–64807
- 28 Nusenu S Y, Wang W Q. Dual-function FDA MIMO radar-communications system employing costas signal waveforms. In: *Proceedings of IEEE Radar Conference*, Oklahoma City, 2018. 0033–0038
- 29 Liu F, Masouros C, Li A, et al. MU-MIMO communications with MIMO radar: from co-existence to joint transmission. *IEEE Trans Wireless Commun*, 2018, 17: 2755–2770
- 30 Liu F, Zhou L, Masouros C, et al. Toward dual-functional radar-communication systems: optimal waveform design. *IEEE Trans Signal Process*, 2018, 66: 4264–4279
- 31 Liu F, Masouros C, Ratnarajah T, et al. On range sidelobe reduction for dual-functional radar-communication waveforms. *IEEE Wireless Commun Lett*, 2020, 9: 1572–1576
- 32 Tsinos C G, Arora A, Chatzinotas S, et al. Joint transmit waveform and receive filter design for dual-function radar-communication systems. *IEEE J Sel Top Signal Process*, 2021, 15: 1378–1392
- 33 Liu R, Li M, Liu Q, et al. Dual-functional radar-communication waveform design: a symbol-level precoding approach. *IEEE J Sel Top Signal Process*, 2021, 15: 1316–1331
- 34 Hassanien A, Amin M G, Aboutanios E, et al. Dual-function radar communication systems: a solution to the spectrum congestion problem. *IEEE Signal Process Mag*, 2019, 36: 115–126
- 35 Hassanien A, Amin M G, Zhang Y D, et al. Dual-function radar-communications: information embedding using sidelobe control and waveform diversity. *IEEE Trans Signal Process*, 2016, 64: 2168–2181
- 36 Hassanien A, Amin M G, Zhang Y D, et al. Phase-modulation based dual-function radar-communications. *IET Radar Sonar Navigation*, 2016, 10: 1411–1421
- 37 Ahmed A, Zhang Y D, Gu Y. Dual-function radar-communications using QAM-based sidelobe modulation. *Digital Signal Process*, 2018, 82: 166–174
- 38 Hassanien A, Aboutanios E, Amin M G, et al. A dual-function MIMO radar-communication system via waveform permutation. *Digital Signal Process*, 2018, 83: 118–128
- 39 Wang X, Hassanien A, Amin M G. Dual-function MIMO radar communications system design via sparse array optimization. *IEEE Trans Aerosp Electron Syst*, 2019, 55: 1213–1226
- 40 Fan W, Liang J, Chen Z, et al. Spectrally compatible aperiodic sequence set design with low cross- and auto-correlation PSL. *Signal Process*, 2021, 183: 107960
- 41 Wu W, Cao Y, Wang S, et al. MIMO waveform design combined with constellation mapping for the integrated system of radar and communication. *Signal Process*, 2020, 170: 107443
- 42 Fan W, Liang J, Li J. Constant modulus MIMO radar waveform design with minimum peak sidelobe transmit beampattern. *IEEE Trans Signal Process*, 2018, 66: 4207–4222
- 43 Wen Z, Yang C, Liu X, et al. Alternating direction methods for classical and ptychographic phase retrieval. *Inverse Problems*, 2012, 28: 115010
- 44 Hassanien A, Vorobyov S A, Khabbazi-basmenj A. Transmit radiation pattern invariance in MIMO radar with application to DOA estimation. *IEEE Signal Process Lett*, 2015, 22: 1609–1613
- 45 Cheng Z, Han C, Liao B, et al. Communication-aware waveform design for MIMO radar with good transmit beampattern. *IEEE Trans Signal Process*, 2018, 66: 5549–5562
- 46 Wu L, Palomar D P. Sequence design for spectral shaping via minimization of regularized spectral level ratio. *IEEE Trans*

- Signal Process, 2019, 67: 4683–4695
- 47 Yu X, Cui G, Yang J, et al. Wideband MIMO radar waveform design. *IEEE Trans Signal Process*, 2019, 67: 3487–3501
- 48 Yu X, Cui G, Yang J, et al. Wideband MIMO radar beampattern shaping with space-frequency nulling. *Signal Process*, 2019, 160: 80–87
- 49 Lan L, Liao G, Xu J, et al. Transceive beamforming with accurate nulling in FDA-MIMO radar for imaging. *IEEE Trans Geosci Remote Sens*, 2020, 58: 4145–4159
- 50 Lan L, Liao G S, Xu J W, et al. Range-angle-dependent beamforming for FDA-MIMO radar using oblique projection. *Sci China Inf Sci*, 2022, 65: 152305
- 51 Liu F, Masouros C, Li A, et al. Robust MIMO beamforming for cellular and radar coexistence. *IEEE Wireless Commun Lett*, 2017, 6: 374–377

Appendix A Convergence proof of Algorithm 2

As $\lim_{t \rightarrow \infty} \boldsymbol{\mu}_i^{(t)} - \boldsymbol{\mu}_i^{(t-1)} = \mathbf{0}$, $\lim_{t \rightarrow \infty} \boldsymbol{\nu}_s^{(t)} - \boldsymbol{\nu}_s^{(t-1)} = \mathbf{0}$, $\lim_{t \rightarrow \infty} \boldsymbol{\xi}_c^{(t)} - \boldsymbol{\xi}_c^{(t-1)} = \mathbf{0}$, $\lim_{t \rightarrow \infty} \boldsymbol{\lambda}_h^{(t)} - \boldsymbol{\lambda}_h^{(t-1)} = \mathbf{0}$, it follows that

$$\lim_{t \rightarrow \infty} \mathbf{y}_i^{(t)} - \mathbf{A}^\dagger(\theta_i) \mathbf{w}^{(t)} = \mathbf{0}, \quad i = 1, \dots, I, \quad (\text{A1})$$

$$\lim_{t \rightarrow \infty} \mathbf{z}_s^{(t)} - \mathbf{A}^\dagger(\vartheta_s) \mathbf{w}^{(t)} = \mathbf{0}, \quad s = 1, \dots, S, \quad (\text{A2})$$

$$\lim_{t \rightarrow \infty} \mathbf{x}_c^{(t)} - \mathbf{A}^\dagger(\theta_c^{\text{com}}) \mathbf{w}^{(t)} = \mathbf{0}, \quad c = 1, \dots, C, \quad (\text{A3})$$

$$\lim_{t \rightarrow \infty} \mathbf{v}_h^{(t)} - \mathbf{A}^\dagger(\theta_h^{\text{eav}}) \mathbf{w}^{(t)} = \mathbf{0}, \quad h = 1, \dots, E. \quad (\text{A4})$$

Besides, since the sequence $\{\mathbf{w}^{(t)}\}$ generated by (38) is closed form, there exists a stationary point \mathbf{w}^* such that $\lim_{t \rightarrow \infty} \{\mathbf{w}^{(t)}\} = \mathbf{w}^*$. Then, the following inequalities can be derived:

$$\begin{aligned} \|\mathbf{y}_i^{(t)}\| &\leq \|\mathbf{y}_i^{(t)} - \mathbf{A}^\dagger(\theta_i) \mathbf{w}^{(t)}\| + \|\mathbf{A}^\dagger(\theta_i) \mathbf{w}^{(t)}\|, \quad i = 1, \dots, I, \\ \|\mathbf{z}_s^{(t)}\| &\leq \|\mathbf{z}_s^{(t)} - \mathbf{A}^\dagger(\vartheta_s) \mathbf{w}^{(t)}\| + \|\mathbf{A}^\dagger(\vartheta_s) \mathbf{w}^{(t)}\|, \quad s = 1, \dots, S, \\ \|\mathbf{x}_c^{(t)}\| &\leq \|\mathbf{x}_c^{(t)} - \mathbf{A}^\dagger(\theta_c^{\text{com}}) \mathbf{w}^{(t)}\| + \|\mathbf{A}^\dagger(\theta_c^{\text{com}}) \mathbf{w}^{(t)}\|, \quad c = 1, \dots, C, \\ \|\mathbf{v}_h^{(t)}\| &\leq \|\mathbf{v}_h^{(t)} - \mathbf{A}^\dagger(\theta_h^{\text{eav}}) \mathbf{w}^{(t)}\| + \|\mathbf{A}^\dagger(\theta_h^{\text{eav}}) \mathbf{w}^{(t)}\|, \quad h = 1, \dots, E. \end{aligned}$$

In this respect, the sequences $\{\mathbf{y}_i^{(t)}\}$, $\{\mathbf{z}_s^{(t)}\}$, $\{\mathbf{x}_c^{(t)}\}$, $\{\mathbf{v}_h^{(t)}\}$ are bounded, and thus there exists a stationary point $\{(\mathbf{w}^{(t)}, \mathbf{y}_i^{(t)}, \mathbf{z}_s^{(t)}, \mathbf{x}_c^{(t)}, \mathbf{v}_h^{(t)})\}$ such that

$$\lim_{t \rightarrow \infty} \{(\mathbf{w}^{(t)}, \mathbf{y}_i^{(t)}, \mathbf{z}_s^{(t)}, \mathbf{x}_c^{(t)}, \mathbf{v}_h^{(t)})\} = \{(\mathbf{w}^*, \mathbf{y}_i^*, \mathbf{z}_s^*, \mathbf{x}_c^*, \mathbf{v}_h^*)\},$$

and

$$\begin{aligned} \mathbf{0} &= \lim_{t \rightarrow \infty} \mathbf{y}_i^{(t)} - \mathbf{A}^\dagger(\theta_i) \mathbf{w}^{(t)} = \mathbf{y}_i^* - \mathbf{A}^\dagger(\theta_i) \mathbf{w}^*, \quad \forall i, \\ \mathbf{0} &= \lim_{t \rightarrow \infty} \mathbf{z}_s^{(t)} - \mathbf{A}^\dagger(\vartheta_s) \mathbf{w}^{(t)} = \mathbf{z}_s^* - \mathbf{A}^\dagger(\vartheta_s) \mathbf{w}^*, \quad \forall s, \\ \mathbf{0} &= \lim_{t \rightarrow \infty} \mathbf{x}_c^{(t)} - \mathbf{A}^\dagger(\theta_c^{\text{com}}) \mathbf{w}^{(t)} = \mathbf{x}_c^* - \mathbf{A}^\dagger(\theta_c^{\text{com}}) \mathbf{w}^*, \quad \forall c, \\ \mathbf{0} &= \lim_{t \rightarrow \infty} \mathbf{v}_h^{(t)} - \mathbf{A}^\dagger(\theta_h^{\text{eav}}) \mathbf{w}^{(t)} = \mathbf{v}_h^* - \mathbf{A}^\dagger(\theta_h^{\text{eav}}) \mathbf{w}^*, \quad \forall h. \end{aligned}$$

Furthermore, $\epsilon^{(t+1)}$, $\eta^{(t+1)}$ derived by (39) and (40) are bounded, which satisfies $\lim_{t \rightarrow \infty} \epsilon^{(t+1)} = \epsilon^*$ and $\lim_{t \rightarrow \infty} \eta^{(t+1)} = \eta^*$ with ϵ^* and η^* being the stationary points.